NAVAL POSTGRADUATE SCHOOL
Monterey, California

THESIS

PREDICTION OF THE PLANE WAVE BEAMFORMED ACOUSTIC ARRIVAL STRUCTURE FOR THE 1992 BARENTS SEA COASTAL TOMOGRAPHY TEST

by

John L. Mykyta

December 1993

Thesis Advisor: Ching-Sang Chiu
Co-Advisor: James H. Miller

URITY CLASSIFICATION OF THIS PAGE

REPORT DOCUMENTATION PAGE

REPORT SECURITY CLASSIFICATION: UNCLASSIFIED	1b. RESTRICTIVE MARKINGS
SECURITY CLASSIFICATION AUTHORITY	3. DISTRIBUTION/AVAILABILITY OF REPORT: Approved for public release; distribution is unlimited
DECLASSIFICATION/DOWNGRADING SCHEDULE	
PERFORMING ORGANIZATION REPORT NUMBER(S)	5. MONITORING ORGANIZATION REPORT NUMBER(S)
NAME OF PERFORMING ORGANIZATION: ceanography Dept. aval Postgraduate School; 6b. OFFICE SYMBOL (if applicable): OC	7a. NAME OF MONITORING ORGANIZATION: Naval Postgraduate School
ADDRESS (City, State, and ZIP Code): onterey, CA 93943-5000	7b. ADDRESS (City, State, and ZIP Code): Monterey, CA 93943-5000
NAME OF FUNDING/SPONSORING ORGANIZATION: ffice of Naval Research; 8b. OFFICE SYMBOL (if applicable): 1125AR	9. PROCUREMENT INSTRUMENT IDENTIFICATION NUMBER
ADDRESS (City, State, and ZIP Code): 00 North Quincy Street rlington VA 22217-5000	10. SOURCE OF FUNDING NUMBERS

PROGRAM ELEMENT NO.	PROJECT NO.	TASK NO.	WORK UNIT ACCESSION NO

TITLE (Include Security Classification)
REDICTION OF THE BEAMFORMED ACOUSTIC RAY ARRIVAL STRUCTURE FOR THE 1992 BARENTS SEA COASTAL TOMOGRAPHY TEST (U)

PERSONAL AUTHOR(S)
ohn L. Mykyta

a. TYPE OF REPORT	13b. TIME COVERED	14. DATE OF REPORT (Year, Month, Day)	15. PAGE COUNT
aster's Thesis	FROM 09/92 TO 09/93	December 1993	46

SUPPLEMENTARY NOTATION: The views expressed in this thesis are those of the author and do not reflect the official olicy or position of the Department of Defense or the United States Government.

COSATI CODES			18. SUBJECT TERMS (Continue on reverse if necessary and identify by block number)
FIELD	GROUP	SUB-GROUP	tomography, eigenray, plane wave, beamformed

ABSTRACT (Continue on reverse if necessary and identify by block number)

In an effort to solve the forward propagation problem associated with the 1992 Barents Sea Polar Front Experiment Tomography Test, the transmission of a 224 Hz pulse signal from a near bottom ound source to a vertical hydrophone array was simulated based on three-dimensional ray theory. Through numerical raytracing, followed by eigenray searches and estimations of ray amplitudes, hases and travel times, the arrival structure as a function of time and elevation angle was onstructed. The simulation was performed for both a two-dimensional and three-dimensional nodeled ocean environment in order to examine the significance of three-dimensional effects. The redicted arrival structures compare well with the observed data. Three-dimensional effects proved o be significant only for the latest arrivals.

DISTRIBUTION/AVAILABILITY OF ABSTRACT	21. ABSTRACT SECURITY CLASSIFICATION
[X] UNCLASSIFIED/UNLIMITED [ ] SAME AS RPT. [ ] DTIC USERS	UNCLASSIFIED
a. NAME OF RESPONSIBLE INDIVIDUAL: hing-Sang Chiu	22b. TELEPHONE (Include Area Code): (408) 656-3239 / 22c. OFFICE SYMBOL: OC/Ci

Approved for public release; distribution is unlimited

PREDICTION OF THE BEAMFORMED ACOUSTIC RAY ARRIVAL STRUCTURE FOR THE 1992 BARENTS SEA COASTAL TOMOGRAPHY TEST

by

John L. Mykyta
Lieutenant, United States Navy
B.S., United States Naval Academy, 1987

Submitted in partial fulfillment of the
requirements for the degree of

MASTER OF SCIENCE IN PHYSICAL OCEANOGRAPHY

from the

NAVAL POSTGRADUATE SCHOOL

December 1993

Curtis A. Collins, Chairman,
Department of Oceanography

ABSTRACT

In an effort to solve the forward propagation problem associated with the 1992 Barents Sea Polar Front Experiment Tomography Test, the transmission of a 224 Hz pulse signal from a near bottom sound source to a vertical hydrophone array was simulated based on three-dimensional ray theory. Through numerical raytracing, followed by eigenray searches and estimations of ray amplitudes, phases and travel times, the arrival structure as a function of time and elevation angle was constructed. The simulation was performed for both a two-dimensional and three-dimensional modeled ocean environment in order to examine the significance of three-dimensional effects. The predicted arrival structures compare well with the observed data. Three-dimensional effects proved to be significant only for the latest arrivals.

TABLE OF CONTENTS

ACKNOWLEDGEMENTS

I would like to thank Professor Ching-Sang Chiu, my thesis advisor and Professor James H. Miller, my co-advisor for all their help, guidance and support throughout the course of this work. Additionally, I extend my sincerest appreciation to Laura Ehret, Stefan Hudson, Chris Miller, and my fellow students Jim Kresge, Phil McLaughlin and Chuck Muggleworth for their innumerable contributions along the way. Finally, a thank you to Dr. Thomas Curtin of the Office of Naval Research who provided funding for the project.

I. INTRODUCTION

A. COASTAL ACOUSTIC TOMOGRAPHY

Ocean tomography is an acoustic method for monitoring the ocean interior. It uses low frequency sound energy to collect information on changes in the ocean temperature and current structure while propagating through a water column. The data collected are in the form of changes in pulse travel times. Inverse techniques are applied to this data to create a best estimate of the unknown ocean structure (Munk and Wunsch, 1979).

A tomography problem consists of two parts: the forward problem, which establishes the physical relationship between the data and the unknown structure; and the inverse problem, which deals with the reconstruction of the unknown environment based on the physical relationships established in the forward problem. The feasibility of using acoustic tomography to monitor the ocean interior depends upon the following requirements (Munk and Wunsch, 1979):

1. Stability
2. Resolvability
3. Identifiability
4. Adequate Signal-to-Noise Ratio

Stable and resolvable multipath arrivals are necessary over successive transmissions in order to derive a useful time series of acoustic travel times. Additionally, identifiability, i.e., association of modeled data to observed data, is needed in order to determine the geometry of the acoustic paths. Signal to noise ratio determines the accuracy of the travel time measurements which, in turn, determines the reliability of the acoustic images of the ocean interior.

In the past, ocean tomography was mainly used for deep ocean monitoring. The adaptation of the deep water technique to shallow coastal waters is the main thrust of a recent collaboration between scientists and engineers at the Naval Postgraduate School and

Woods Hole Oceanographic Institution (Chiu, et al., 1993(a) and Miller, et al., 1993). Relative to deep water propagation, the multipath arrivals from a pulse excitation in shallow water tend to overlap in time, making it difficult to resolve them individually with the typical receiver configurations used for open ocean applications. In the 1992 Barents Sea Coastal Tomography Test, Chiu, et al. (1993(a)) and Miller, et al. (1993) successfully used a vertical line array receiver and beamforming techniques to overcome this difficulty. Additionally, Chiu, et al. (1993(a)) developed new hybrid ray-mode inverse technique to provide optimal sound speed maps with minimum mean square errors. As a result, the Barents Sea Polar Front Experiment has successfully addressed the requirements for coastal applications of acoustic tomography.

B. BARENTS SEA POLAR FRONT EXPERIMENT

The Barents Sea Polar Front Experiment (BSPFEX) was conducted in August 1992 by researchers from the Naval Postgraduate School (NPS), Woods Hole Oceanographic Institution (WHOI), and Science Applications International Corporation (SAIC), (Barents Sea Polar Front Group, 1992). BSPFEX, conducted within an 80 X 90 km rectangle centered 50 km east of Bear Island, utilized both acoustical tomography and traditional oceanographic techniques to study the Barents Sea Polar Front.

The Barents Sea is bordered to the north by Spitzbergen and Franz Joseph Land, to the south by Scandinavia and Russia, to the east by Novaya Zemlya and is open to the west. Currents in the region transport water of both Arctic and Atlantic origin that converge at the Barents Sea Polar Front. The colder Arctic water flows from the north, while the warmer Atlantic water flows in from the southwest. These water masses have vastly different temperature and salinity characteristics (see Table 1), and the confluence of these flows results in complex vertical and horizontal structure within the frontal zone. Figure 1 depicts Loeng's (1991) model of the regions occupied by the major water masses. The

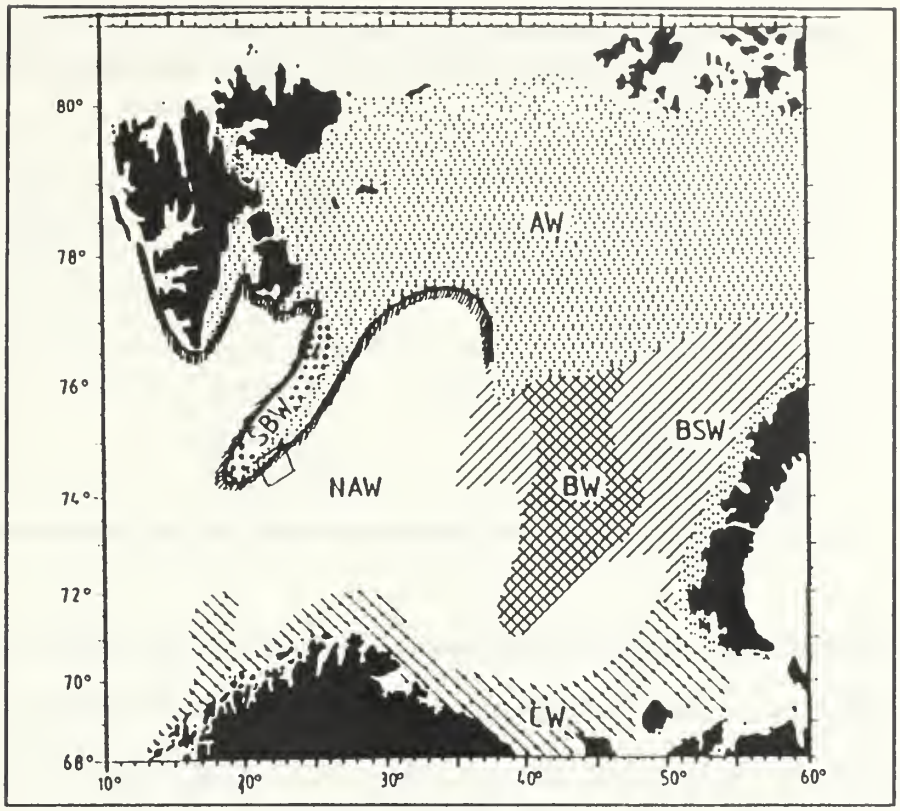

Figure 1. Barents Sea water masses (Loeng, 1991)

abbreviations are as follows: Arctic Water (AW), North Atlantic Water (NAW), Svalbard Bank Water(SBW), Barents Sea Water (BSW), and Bottom Water (BW). The area occupied by BSPFEX is also indicated in the figure by a rectangle.

The physical oceanographic characteristics of the experimental region have a significant impact on sound propagation. The region is shallow, with an average depth of 224 m. The bottom, appreciably rough in some areas, consists of thin sediments overlying hard rock. The range dependence of the bathymetry and sound speed, coupled with the shallowness of the water depth can result in complex sound refraction and boundary interactions (Elliot, 1992). The effects of these environmental factors on sound propagation will be discussed further in Chapter II.

Table 1: BARENTS SEA WATER MASSES (Leong, 1991)

Major Types	T(^{0}C)	S(psu)
Arctic Water (AW)	<0.5	34.2 - 34.0
North Atlantic Water (NAW)	-0.5 to 2.0	34.8 - 35.0
Local Variants	**T(^{0}C)**	**S(psu)**
Svalbard Bank Water (SBW)	1 .0 to 3.0	< 34.4
Bottom Water (BW)	<-1.5	> 35.0
Barents Sea Water (BSW)	-1.5 to 2.0	34.7 - 35.0
Polar Front Water (PW)	-0.5 to 2.0	34.8 - 35.0

The Barents Sea Polar Front Experiment consisted of three major components, a physical oceanographic investigation of the polar front, a coastal tomography test, and an acoustic propagation study. The scientific objectives of the coastal tomography test are summarized below (Chiu, et al., 1993):

1.To study the dynamics of the front near Bear Island by mapping its spatial and temporal variability.

2. To assess the performance of a new coastal acoustic tomography system in mapping frontal features.

Figure 2 shows the experimental configuration for the test. The tomography system included a 224 Hz source (A), a vertical array of sixteen hydrophones (B), and two 400 Hz transceivers (C and D). The placements of the tomographic elements are summarized in Table 2. This forward modeling work focus solely upon the propagation path between the 224 Hz source (A) and the vertical hydrophone array (B).

The 224 Hz source was moored 20 m above the sea floor. The vertical array consisted of 16 evenly spaced hydrophones at 10 m apart with the bottom hydrophone being situated 4.82 m

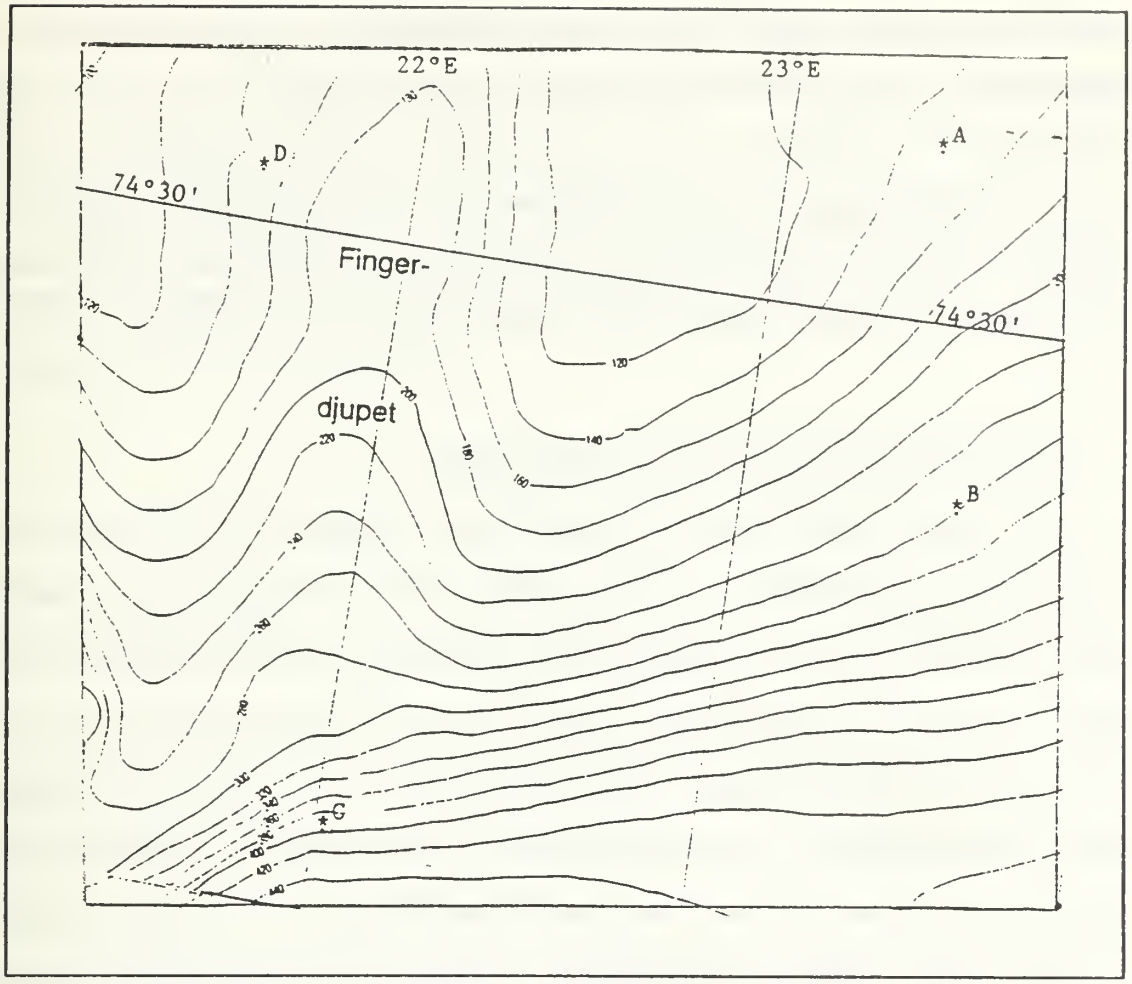

Figure 2. Experimental configuration for tomography transmission test (Norsk, 1986).

Table 2: LOCATIONS OF ACOUSTIC ELEMENTS

Mooring	Type	Lat (^{0}N)	Lon(^{0}E)
A	Source	74.63	23.40
B	Hydrophone Array	74.32	23.55
C	Transceiver	74.08	22.00
D	Transceiver	74.55	21.72

above the sea floor. Both ray and mode propagation models are required for the identification of the plane wave and modal beamformed acoustic arrivals and the subsequent inversion of the travel time data. This study focuses on the use of a three-dimensional ray propagation model for the prediction of the beamformed ray arrival structure. The modeling of the modal arrival structure is currently in progress (Chiu, et al., 1993(a)). The beamforming techniques used are discussed in Miller, et al., (1993), and the hybrid ray-mode inversion method used is outlined in Chiu, et al., (1993(a)).

C. THESIS OBJECTIVES AND APPROACHES

The objective of this thesis is to examine and establish the ray forward problem associated with the BSPFEX Coastal Tomography Test. A three dimensional acoustic ray theory approach was used to simulate the transmission of the 224 Hz tomographic pulse signal from the near bottom sound source (A) to the vertical receiver array (B), approximately 34 km downrange. To develop a prediction of the plane wave beamformed arrival structure a dense set of rays was first traced. Based on these rays, eigenrays and their amplitudes and phases were then determined. The predicted arrival structure, as a function of time and angle, is the key for identifying the observed arrivals. The simulation was done for both a three-dimensional (3-D) and a two-dimensional (2-D) modeled ocean environment in order to examine the importance of the 3-D effects.

The model used for the ray tracing was the Hamiltonian Ray Tracing Program for the Ocean (HARPO). The input ocean environments were mathematical models based on a bathymetric chart of the region (Norsk, 1986) and derived sound speed values from seventy-two evenly spaced Conductivity/Temperature/Depth (CTD) stations within the test area. The estimation of eigenrays and the associated arrival structure for both the 2-D and 3-D environments was accomplished using a MATLAB program that operates on the rays traced by HARPO.

D. THESIS OUTLINE

The remainder of this thesis consists of four chapters. Chapter II discusses acoustic ray theory, the ray tracing program HARPO, and a description of the methods used to calculate the amplitude and phase of the individual arrivals.

In Chapter III, the methods used to model the environments for input into HARPO are described. Chapter IV presents and discusses the simulated arrival structure and Chapter V presents the conclusion of this study.

II. ACOUSTIC RAY THEORY MODELING

A. INTRODUCTION

The model used for the numerical raytracing was the NOAA Hamiltonian Acoustic Raytracing Program for the Ocean (HARPO) (Jones, et al., 1986). HARPO is a (3-D) FORTRAN code that determines acoustic path solutions by integrating Hamilton's equation. Jones, et al. (1986) have provided a complete description of the algorithm. For input, HARPO requires a continuous representation of a 3-D sound speed field, and a continuous 2-D representation of the upper and lower reflecting surfaces, i.e., the sea surface and bathymetry. Gridded bathymetric and sound speed data can be made continuous by FORTRAN subroutines external to HARPO through the use of empirical orthogonal functions (EOFs) and splines (Chiu, et al., 1993(b)). HARPO itself does not provide a prediction of the multipath arrival structure, but a MATLAB program 'raystructure.m' developed by Chiu (1993) can be applied to HARPO output files for the searches of eigenrays and the computation of ray amplitudes and phases based on estimates of ray tube spreading and losses and phase modifications due to boundary interactions.

B. HAMILTONIAN RAY TRACING

Acoustic energy travels in the form of compressional waves, but in the high frequency approximation these waves behave like particles whose paths are described by integrating a differential form of the wave equation. HARPO borrows Hamilton's equation from quantum mechanics and applies it to sound propagation. The general form of Hamilton's equation is:

$$\frac{dp_i}{dt} = \frac{\partial H}{\partial q_i} \qquad i = 1, 2, 3$$
$$\frac{dq_i}{dt} = \frac{\partial H}{\partial p_i} \qquad i = 1, 2, 3 \tag{1}$$

where the Hamiltonian function $H(p_1,p_2,p_3;q_1,q_2,q_3)$ represents a system's total energy with respect to a generalized coordinate system p, and momenta q. The coordinate system used by HARPO is spherical polar, and for acoustic applications, q represents the wave number vector. Therefore, upon specifying initial values for Equation (1), solutions are obtained by integrating the system of differential equations. The form of the Hamiltonian in sound propagation is:

$$H(p_i, q_i) = \omega^2 - c(p_i)\, q^2 \tag{2}$$

where ω represents the angular wave frequency, $c(p_i)$ is the sound speed field, and q^2 is the magnitude squared of the wave number vector (Jones et al., 1986).

C. ARRIVAL STRUCTURE ESTIMATION

Within the ray theory framework, the received signal, $r(t)$, at a single phone can be approximated as:

$$r(t) \cong \sum_{j=1}^{N} a_j s(t - t_j)\, exp(-i\phi_j) \tag{3}$$

where N is the number of eigenrays, $s(t)$ is the signal emitted by the source, and a_j, ϕ_j, and t_j respectively represent the amplitude, phase shift and travel time for each eigenray arrival.

The travel time, or path integral of sound slowness, was calculated in HARPO as each ray was traced. The MATLAB program' raystructure.m' was used to find eigenrays and

determine their respective amplitudes and phases in order to develop an estimate of the ray arrival structure using Equation (3).

For each eigenray, the phase shift was modified for each boundary interaction and turning point (caustic interaction). For each surface reflection, the phase was reduced by π. For a turning point (caustic interacion), it was reduced by $\pi/2$, and for a bottom interaction, the phase of the reflection coefficient evaluated at the ray angle incident on the bottom was added.

Eigenray amplitude was calculated by correcting for losses due to ray tube spreading, surface scattering and bottom reflection. A description of these factors and the equations used for the correction are given below.

1. Ray Tube Spreading

Spreading loss is the geometrical effect that represents the weakening of a sound signal as it spreads outward from a source (Urick, 1983). This weakening of the signal is the result of the focusing or defocusing of adjacent rays as they propagate down range. The transmission equation for ray tube spreading for a non-absorbing medium (Clay and Medwin, 1977) is:

$$P^2 = P_0^2 R_0^2 \frac{\Delta\theta c |\cos\theta_0|}{rhc_0|\cos\theta|} \tag{4}$$

where R_o represents a reference radius, P_o is the pressure at R_o , c_0 is the sound speed at R_o, and θ_0 is the grazing elevation angle at R_o. P, c, and θ respectively represent the pressure, sound speed and angle at range r. The vertical separation between adjacent rays at range r is represented by h, and $\Delta\theta$ is the increment between the initial launch angles of the adjacent rays. The MATLAB program 'raystructure.m' uses this equation to calculate the effect of ray tube spreading on relative magnitude.

2. Surface Scattering

The shallowness of the Barents Sea plays a significant role in sound propagation in that many rays interact with the surface. The sea surface can both reflect and scatter sound. For a smooth sea, the magnitude of the reflection coefficient (ratio of reflected pressure to incident pressure) is unity. For a rough sea surface however, because some of the energy is scattered, the magnitude of the coherent reflection coefficient is less than unity and decreases with increasing wave height (Brekhovskikh, et al.,1982). This coherent reflection coefficient is dependent on the Rayleigh parameter:

$$R = k\sigma\sin\theta \tag{5}$$

where k is the wave number, σ represents the root mean square displacement of a rough surface, and θ is the grazing angle relative to the horizontal. The magnitude of the coherent reflection coefficient, R_{Sfc}, for an irregular surface can be expressed as (Brekhovskikh, et al.,1982):

$$R_{Sfc} = exp\,(-2R^2) \tag{6}$$

The method described above was used in 'raystructure.m' to include surface scattering losses.

3. Bottom Loss

Bottom interaction can result in a loss of acoustic energy due to both scattering of energy out of the ray tube and the transmission of some of the energy into the bottom. This energy loss can be parameterized by the reflection coefficient at the bottom. If a plane wave is incident on a boundary of two fluids with density ρ_1 and ρ_2, and sound speed c_1 and c_2, at an angle of θ_1, then the smooth interface reflection coefficient (Clay and Medwin, 1977) can be expressed as:

$$R_{Bot} = \frac{\rho_2 c_2 \cos\theta_1 - \rho_1 c_1 \cos\theta_2}{\rho_2 c_2 \cos\theta_1 + \rho_1 c_1 \cos\theta_2} \tag{7}$$

where, by Snell's law:

$$\theta_2 = \text{asin}\left(\frac{c_1}{c_2}\sin\theta_1\right) \tag{8}$$

The program 'raystructure.m' calculates the bottom reflection coefficient in this manner. A bottom sound speed of 3200 m/s and a bottom density of 2700 kg/m^3 were used in this simulation. Bottom scattering loss was assumed to be negligible and therefore not modeled.

III. MODELING THE BARENTS SEA ACOUSTIC ENVIRONMENT

A. GENERAL

Environmental input models for the simulation of the acoustic ray arrival structure were developed using data that provided an adequate description of the bathymetry and sound speed fields. The accuracy of the input models used to describe the ocean environment determine the accuracy in the calculation of sound propagation solutions. A physical oceanographic description of the experimental region is given in Chapter I. In this chapter, the construction of the mathematical environmental models input into HARPO is discussed.

B. SOUND SPEED FIELD

The 3-D sound speed field was developed using measured sound speed profiles from 72 CTD casts. The locations of these CTD stations, occupied during the first ship survey in the BSPFEX, are shown in Figure 4. Each measured profile was first extended to a uniform depth and then interpolated to provide data at a two meter spacing in the vertical direction. Because the focus of this study is on the propagation path between the 224 Hz source and the vertical hydrophone array, the modeled region was chosen to be a 36 x 20 km^2 area occupied by the five tracks shown in Figure 5. Each track is 36 km long with 5 km horizontal spacing between them. Using a horizontal inverse distance technique, a value for sound speed was interpolated every kilometer along each track for every two meters in depth. The resulting profiles were further smoothed vertically using an eleven point hamming filter. This is required to eliminate unrealistic ray chaos resulting from the break down of the ray approximation in the presence of fine structure. Figure 6 shows the sound speed profiles from the four CTD stations located along the line of sight path between the source and the array. The interpolated and smoothed profiles for the same vertical cross section are depicted in Figure 7. A contour plot of the sound speed field along the track between the 224 Hz source and the vertical array is provided in Figure 8.

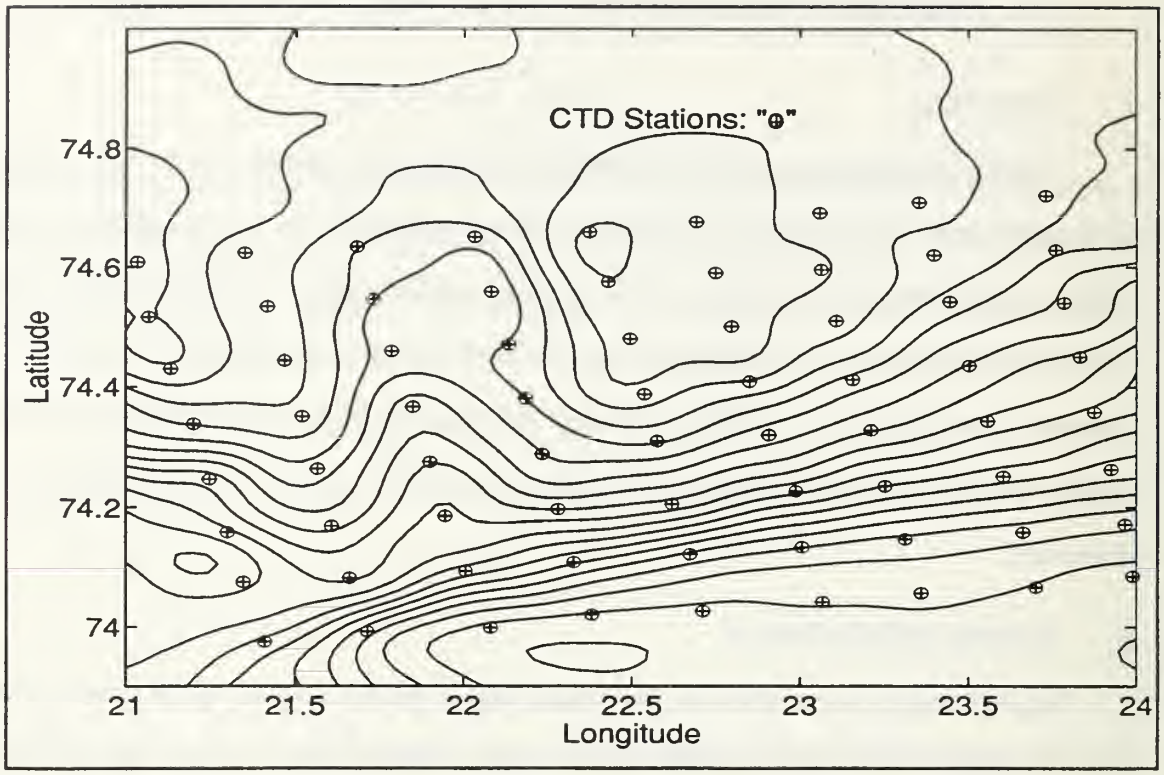

Figure 4. Barents Sea Polar Front Experiment CTD locations.

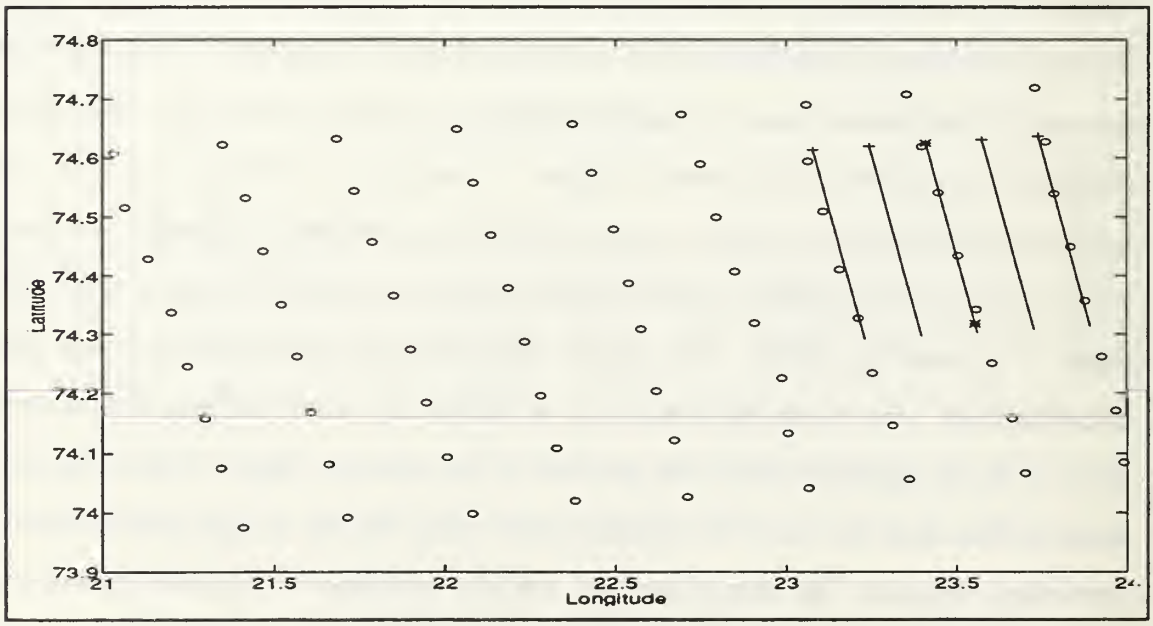

Figure 5. The geographic region used in the environmental input models is represented by the five tracks shown here. Each track is 36 km long with 5 km separation between them.

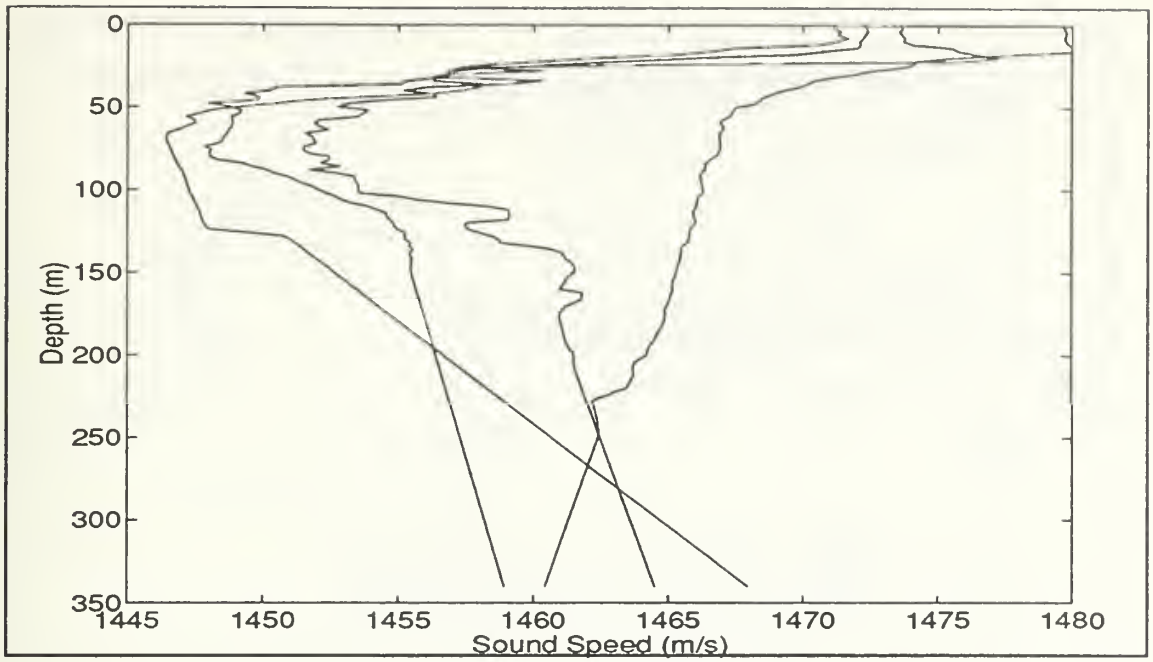

Figure 6. Sound speed profiles from the four CTD stations along the line of sight between the source and receiver.

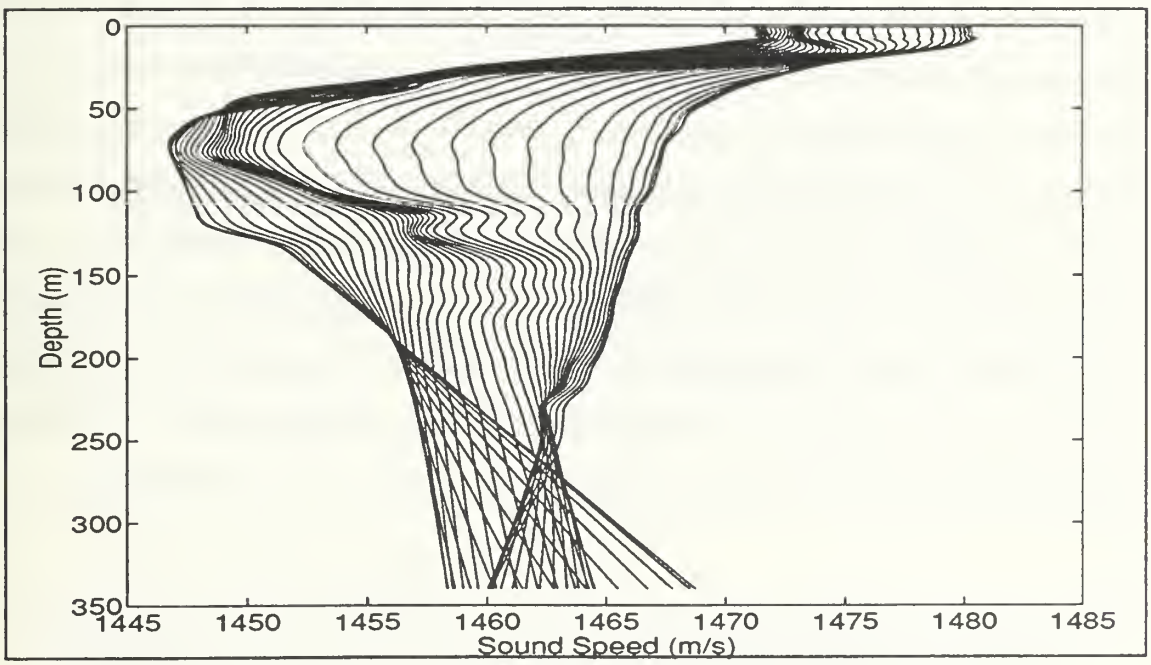

Figure 7. Interpolated and filtered sound speed profiles along the line of sight between the source and receiver.

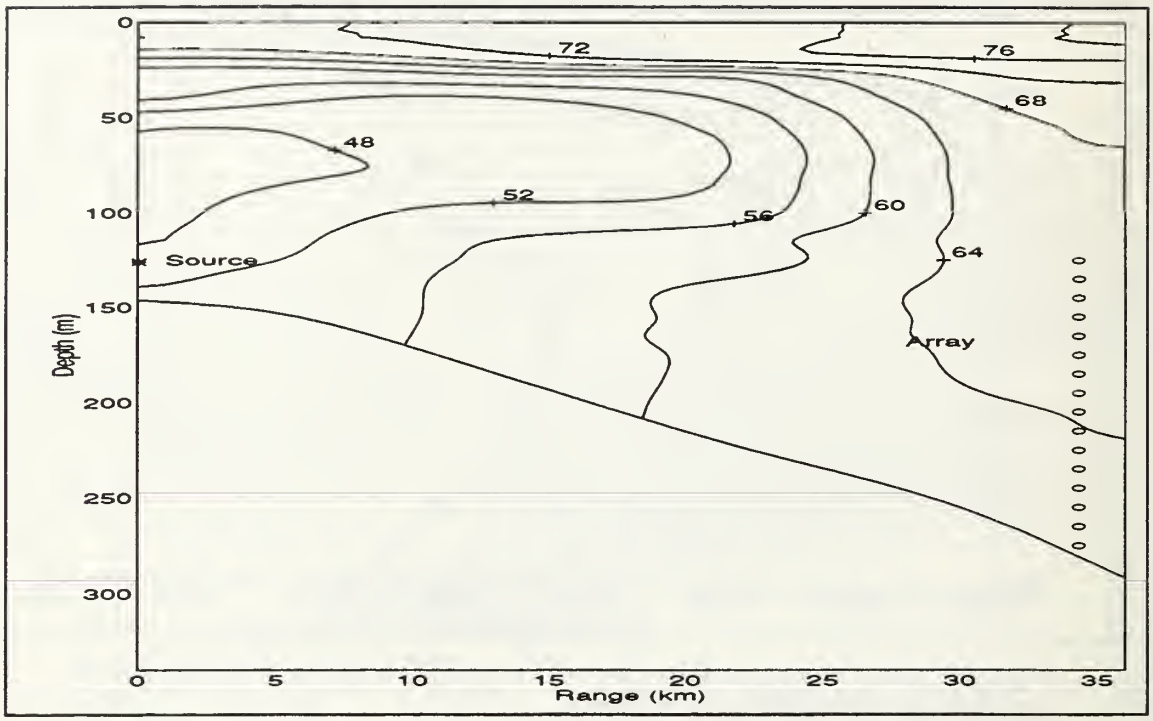

Figure 8. Sound speed contour along the line of sight between the source and receiver. (+1400 m/s)

Figure 9 shows the sound speed contours along each track. Note, from Figure 9, that to the east of the line of sight track lies warmer water with a higher sound speed which will tend to refract sound towards the west. Finally, the gridded sound speed data along the five tracks was made continuous for input into HARPO through the use of empirical orthogonal functions (EOFs) and splines using two FORTRAN subroutines 'gridder.f' and 'cgrid.f' (Newhall, et al., 1987). To determine an adequate number of EOFs needed to accurately represent the actual sound speed field, a MATLAB program 'eof.m' (Chiu, 1993) was used, calculating the maximum error associated with a given number of EOFs. To achieve an acceptable error of 10^{-2}m/s, sixteen EOFs were used for the 3-D environment.

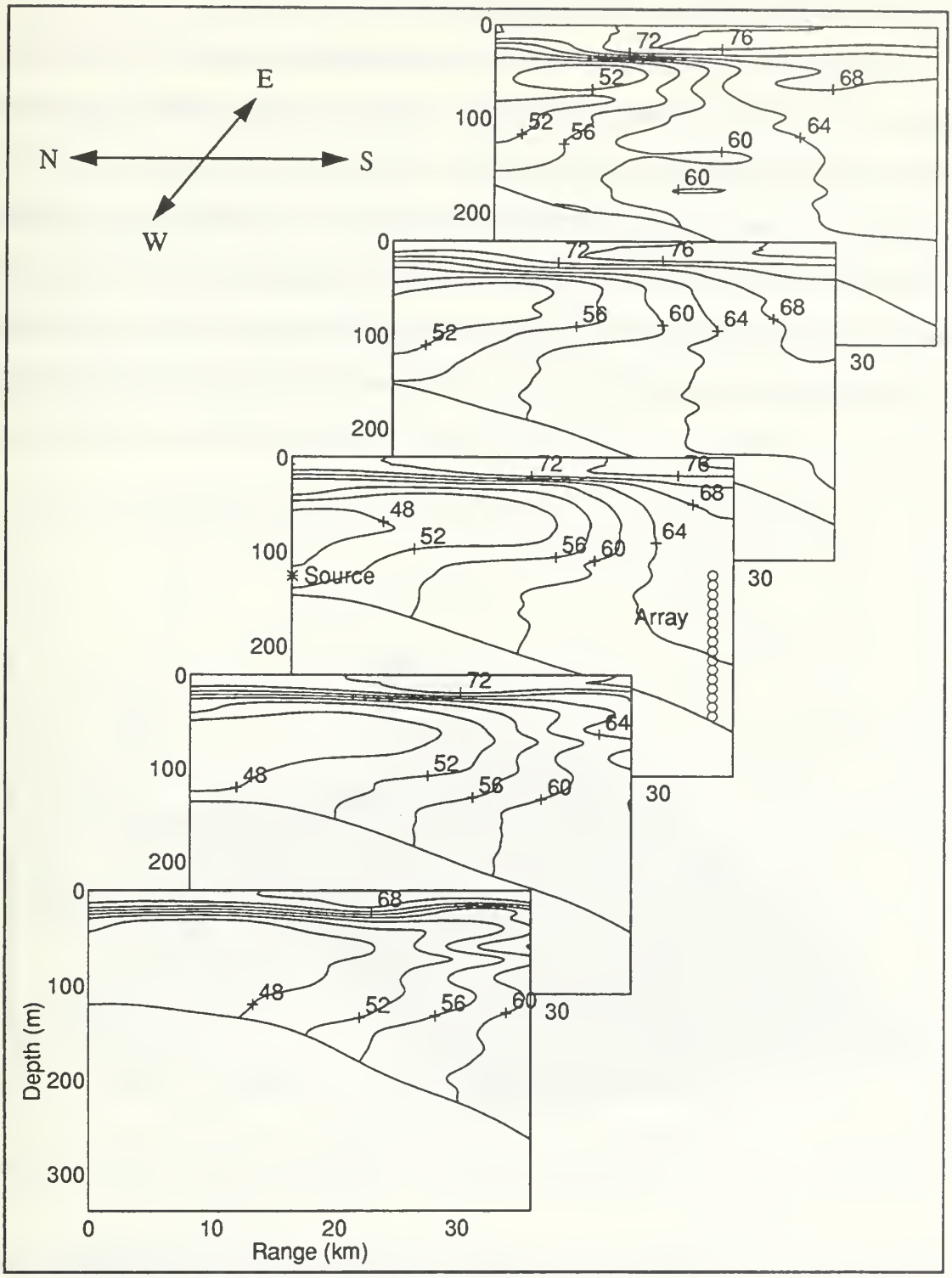

Figure 9. Sound speed contours (+ 1400 m/s) along each track depicted in Figure 5. These contours represent the three dimensional sound speed field used for input to HARPO.

C. BATHYMETRY AND SEA SURFACE

The bathymetry input for HARPO was taken from the chart shown in Figure 2 (Norsk,1986). The region bounded by 21.00 E, 24.00 E, 73.90 N and 74.80 N was gridded into 76 subdivisions on each side, providing a 0.45 km resolution in the longitudinal direction and 0.9 km resolution in the latitudinal direction. Water depths were read directly off the chart at those grid points. Additionally, Acoustic Doppler Current Profiler (ADCP) data provided depths along the track. These two sets of data were merged to provide a high resolution bathymetry model for the region. The resulting bathymetry contours are shown in Figure 10. Because the modeled environment provided such high resolution, it was

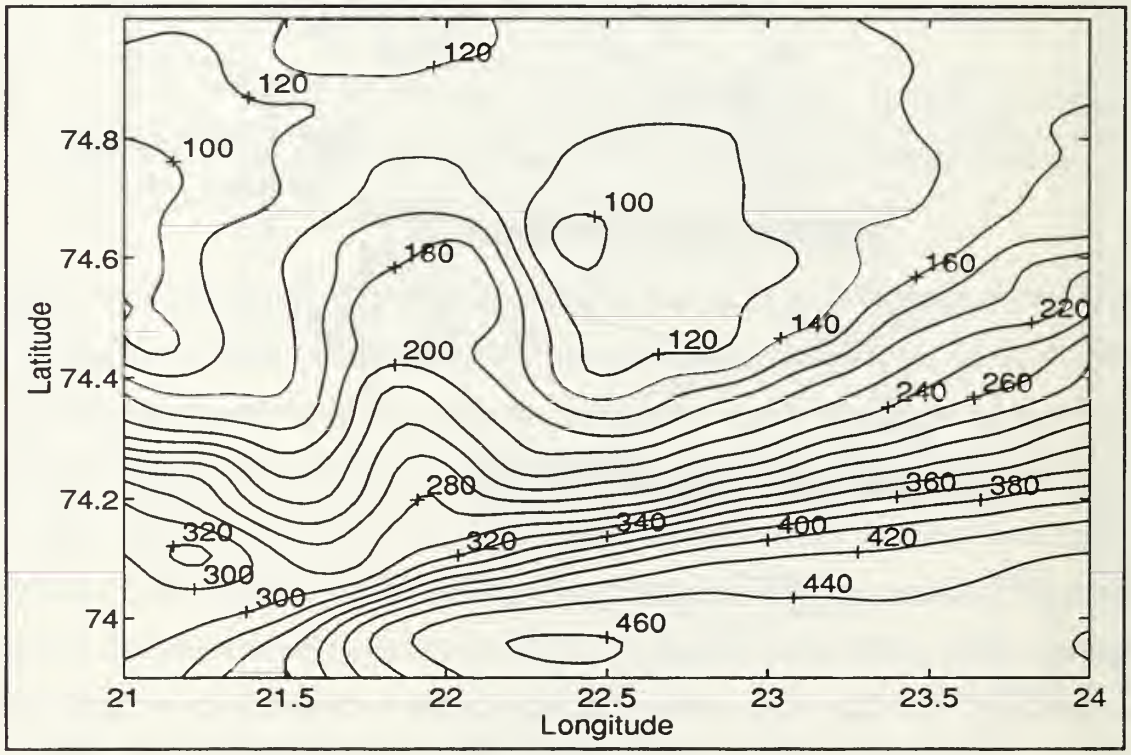

Figure 10. Contour of bathymetry model used as input for HARPO (depth in meters).

necessary to smooth it using a low-pass filter to eliminate ray chaos. Similar to the case of the sound speed field, the input bathymetry field was reduced to a size of 36 x 20 km^2 and

regridded to one kilometer resolution in the latitudinal direction and five kilometer resolution in the longitudinal direction using linear interpolation. A 3-D view of the input bathymetry model is shown in Figure 11. Superimposed on Figure 11 are the locations of the 224 Hz source and the hydrophone array as well as a bottom interacting ray path. Note that the depth increases to the southeast which will tend to steer bottom interacting rays in that direction, counteracting the westward refracting effect of the sound speed field. Using two other FORTRAN subroutines 'tgridder.f' and 'bottom.f' (Newhall, et al., 1987), this gridded input was splined to provide a continuous bathymetry representation for use in HARPO.

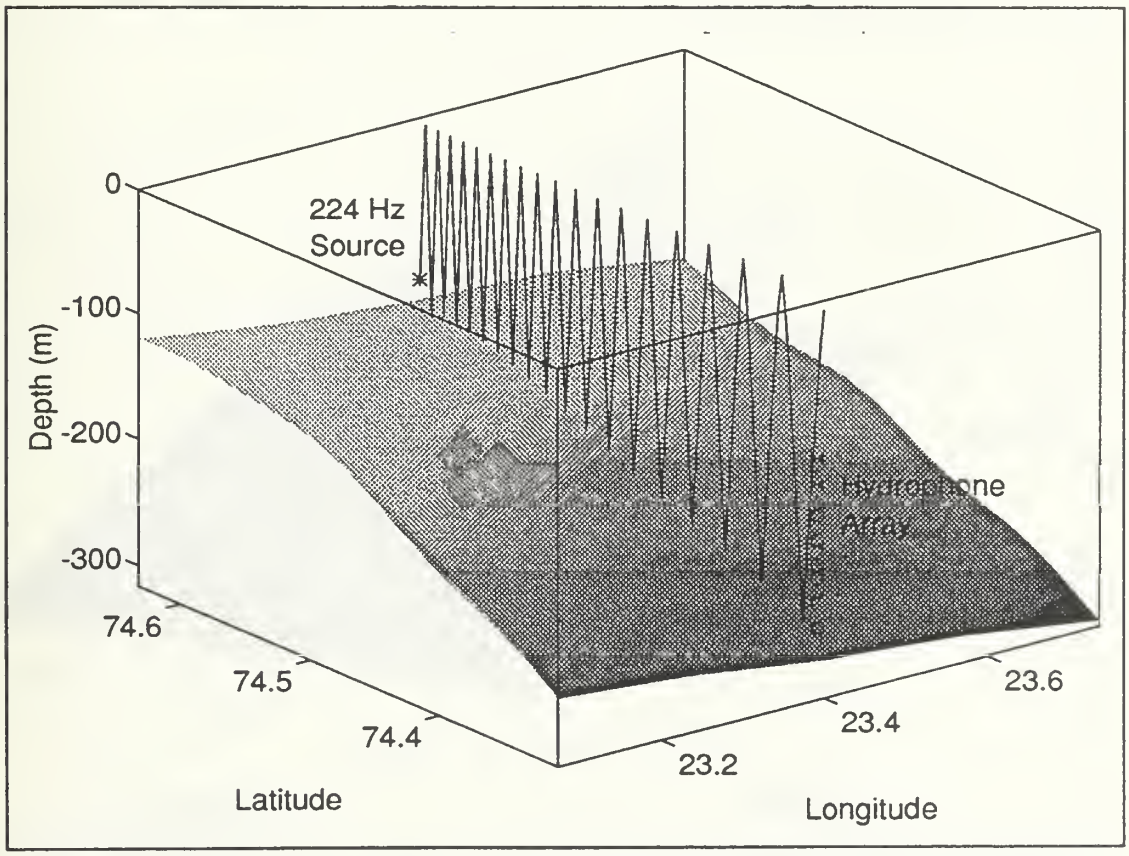

Figure 11. Three dimensional representation of the region of study. Superimposed on this figure are the locations of the 224 Hz source and the hydrophone array as well as a bottom interacting ray path.

regridded to one kilometer resolution in the latitudinal direction and five kilometer resolution in the longitudinal direction using linear interpolation. A 3-D view of the input bathymetry model is shown in Figure 11. Superimposed on Figure 11 are the locations of the 224 Hz source and the hydrophone array as well as a bottom interacting ray path. Note that the depth increases to the southeast which will tend to steer bottom interacting rays in that direction, counteracting the westward refracting effect of the sound speed field. Using two other FORTRAN subroutines 'tgridder.f' and 'bottom.f' (Newhall, et al., 1987), this gridded input was splined to provide a continuous bathymetry representation for use in HARPO.

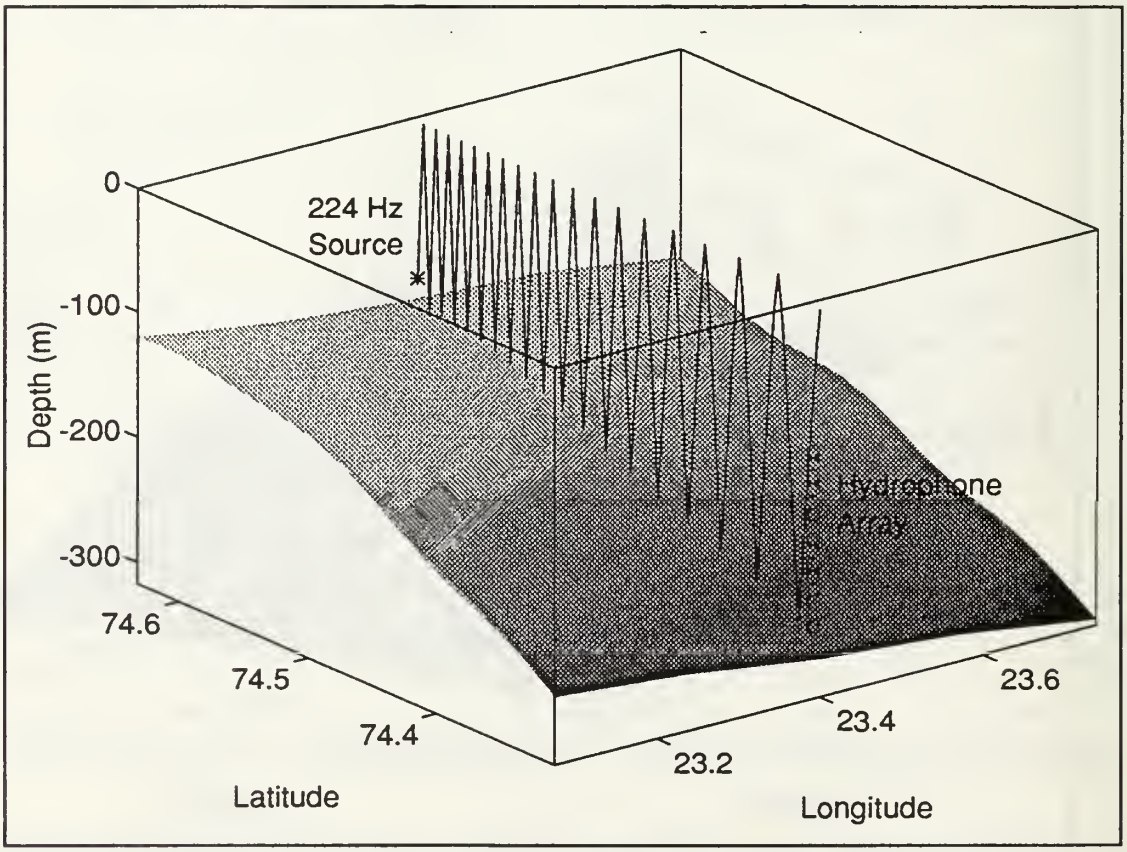

Figure 11. Three dimensional representation of the region of study. Superimposed on this figure are the locations of the 224 Hz source and the hydrophone array as well as a bottom interacting ray path.

The sea surface was modeled as a sphere concentric with the earth with a radius of 6360.481 km.

D. TWO DIMENSIONAL ENVIRONMENT

The 2-D environment was created by substituting the line of sight bathymetry and sound speed profiles into each of the five tracks. Because a smaller number of initial sound speed profiles were used to create this environment, only six EOFs were necessary to achieve the same accuracy as the 3-D case.

IV. SIMULATION RESULTS AND ANALYSIS

A. INTRODUCTION

In simulating the propagation of the 224 Hz tomographic signal from the near bottom source through the Barents Sea Polar Front to the vertical hydrophone array, rays were traced for launch angles between 0.00^{o} and 40.00^{o} at 0.025^{o} increments for both the 2-D and 3-D modeled environments. Eigenrays and their amplitudes, phase shifts and travel times were then estimated for constructing the arrival structure.

B. RAY PATH GEOMETRY

All rays were launched along a constant azimuth and traced to a range of 34.32493 km. Wavefront corrections were applied to ray path length, arrival time and arrival depth. Because of the downward refracting sound speed profile (Figure 6), many of the rays launched at shallow and intermediate grazing angles were refracted-bottom-reflected (RBR). Figure 12 shows the rays launched at 5.00^{o} for both the 2-D and 3-D cases. In both cases, the first ray to interact with the surface was launched at 10.05^{o}. These rays are depicted in Figure 13. The first ray to be completely surface-reflected and bottom-reflected was the 13.35^{o} ray for both the 2-D and 3-D cases. Figure 14 shows these rays. The 3-D environment introduced horizontal refraction into ray path geometries. As expected, those rays launched at shallow angles had minimal bottom interactions and were driven mainly by the sound speed field. Due to the warmer water to the east, these rays were refracted westward. Those rays launched at steeper grazing angles underwent numerous bottom interactions and were steered eastward by the bathymetry. Figure 15 shows the horizontal refraction of selected rays.

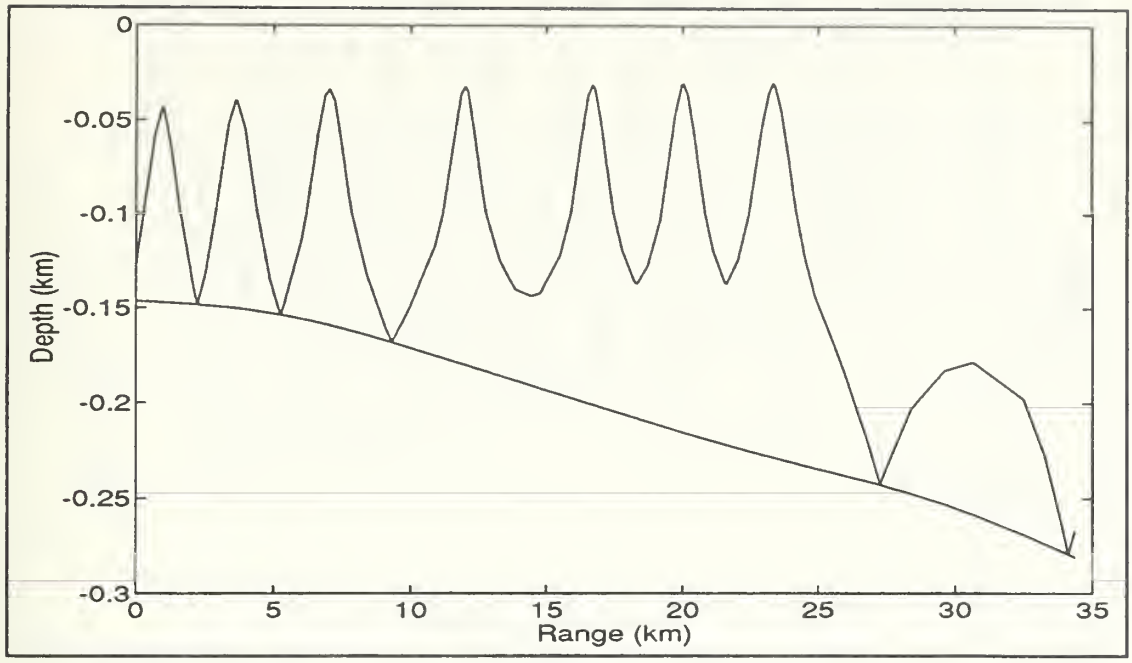

(a)

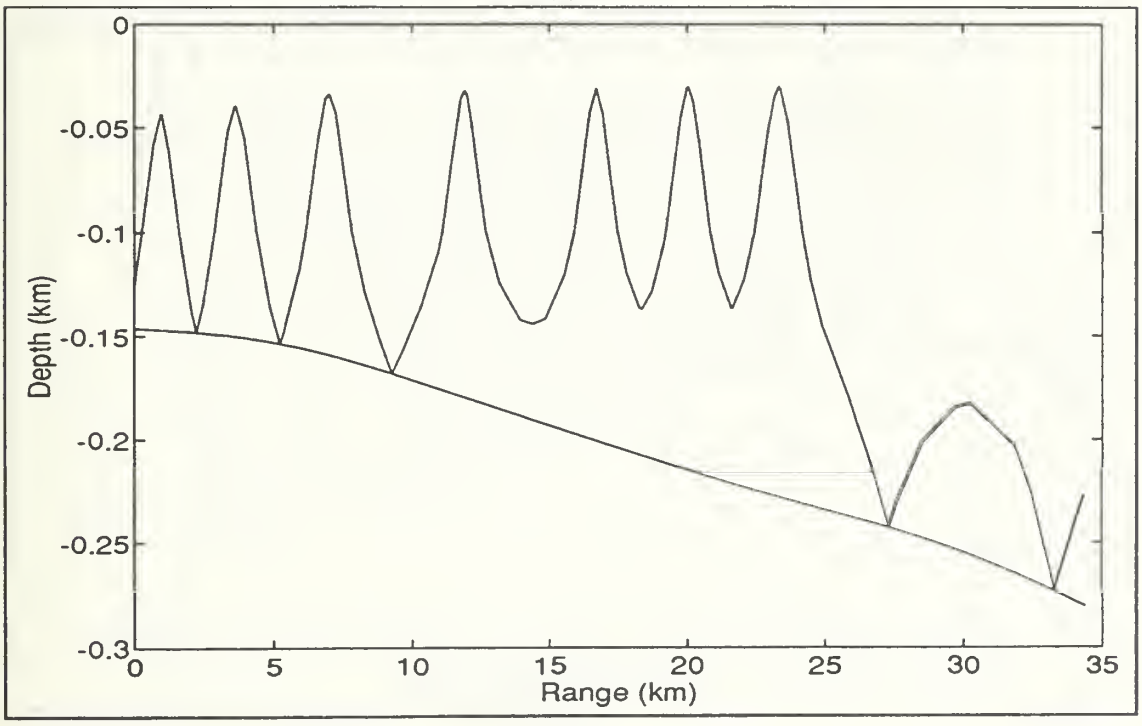

(b)

Figure 12. Path geometry for the ray launched at 5^{o} for (a) the 2-D environment and (b) the 3-D environment.

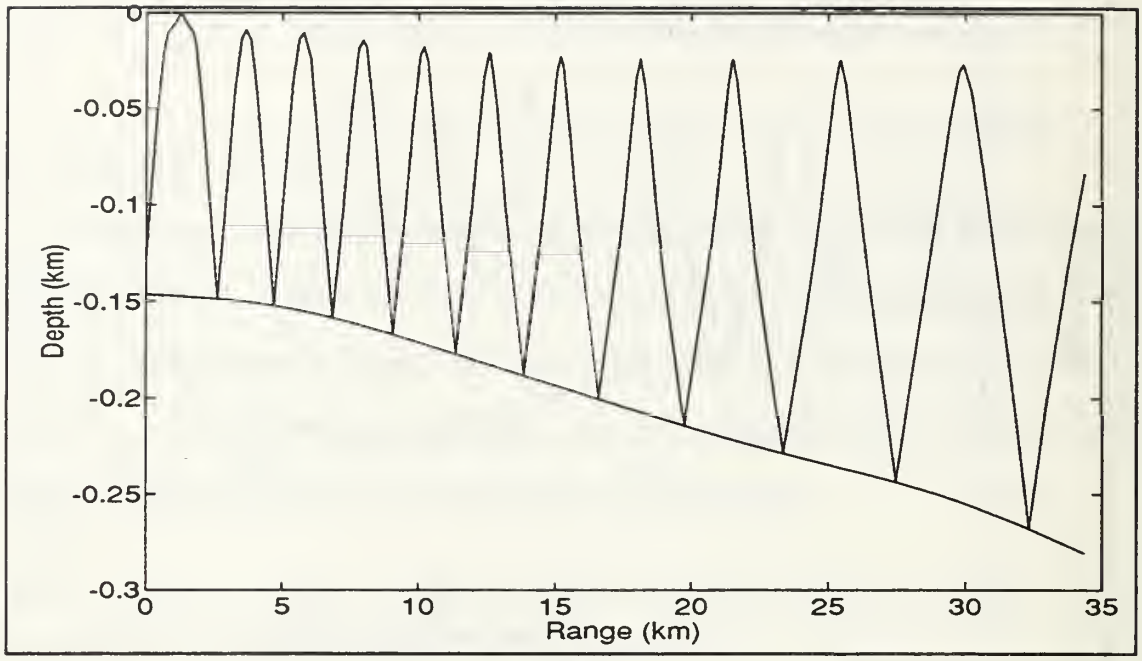

(a)

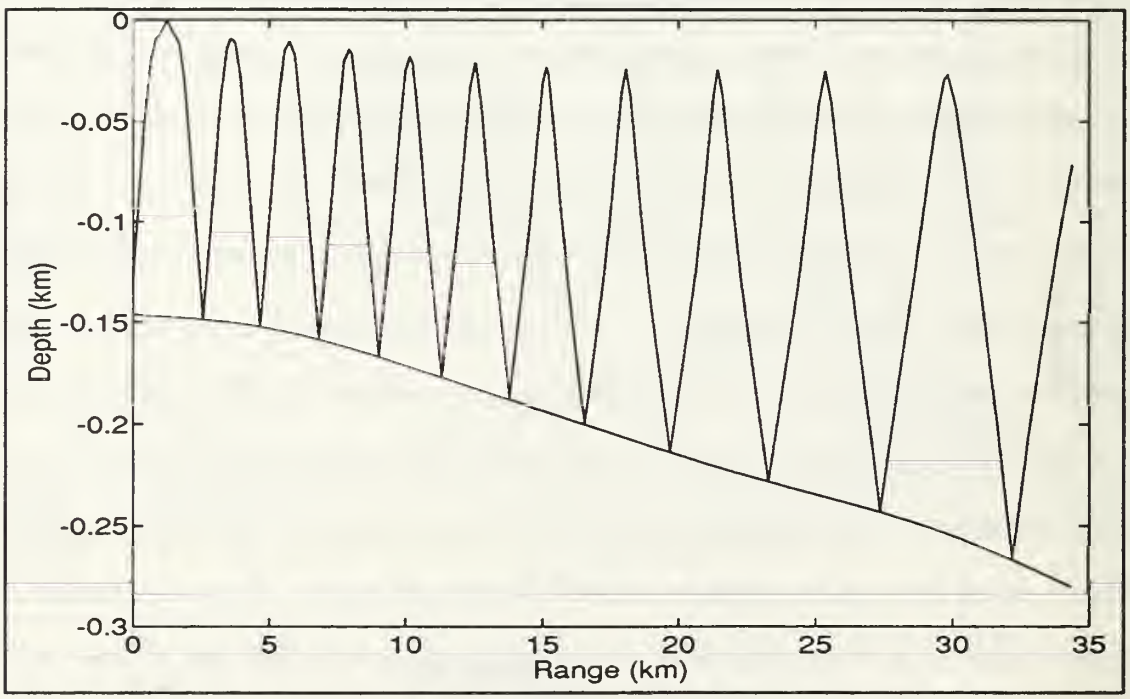

(b)

Figure 13. Path geometry of the ray launched at 10.05^{o} for (a) the 2-D environment and (b) the 3-D environment.

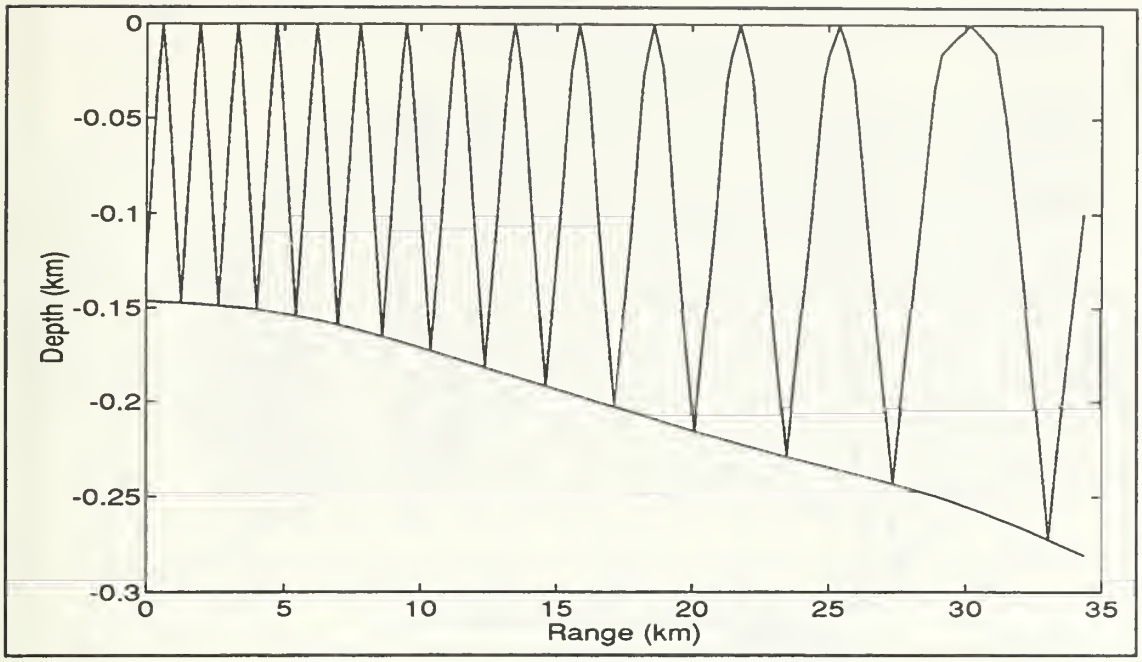

(a)

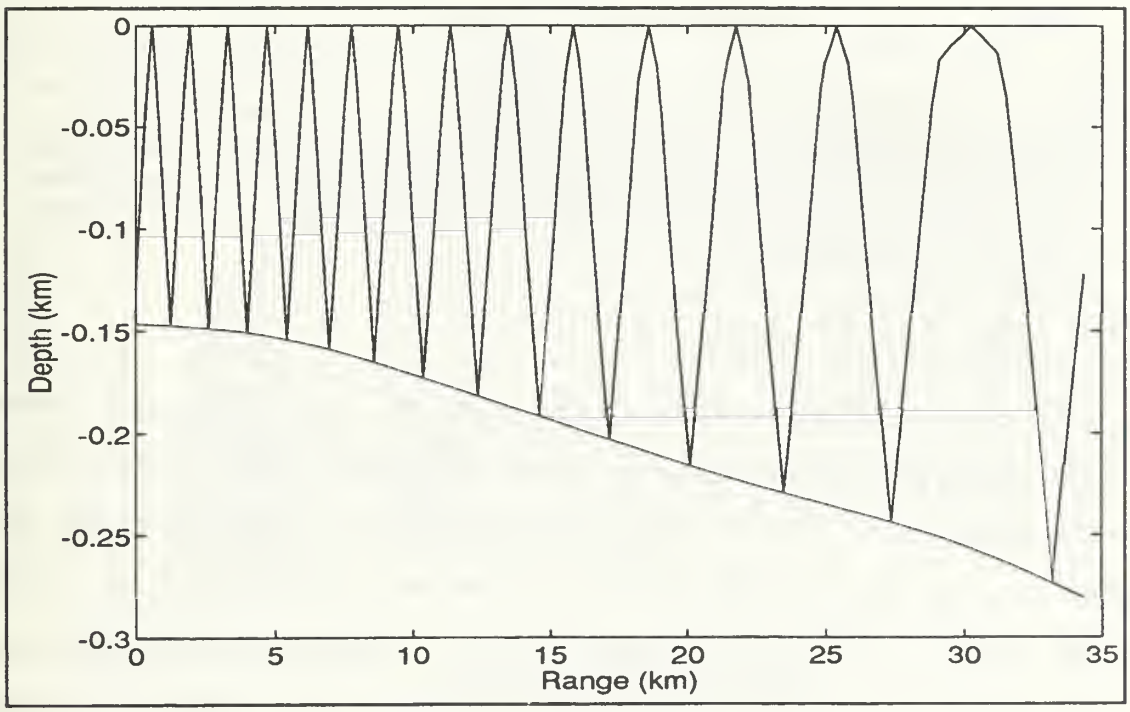

(b)

Figure 14. Path geometry of the ray launched at 13.35^{o} for the (a) 2-D environment and (b) the 3-D environment.

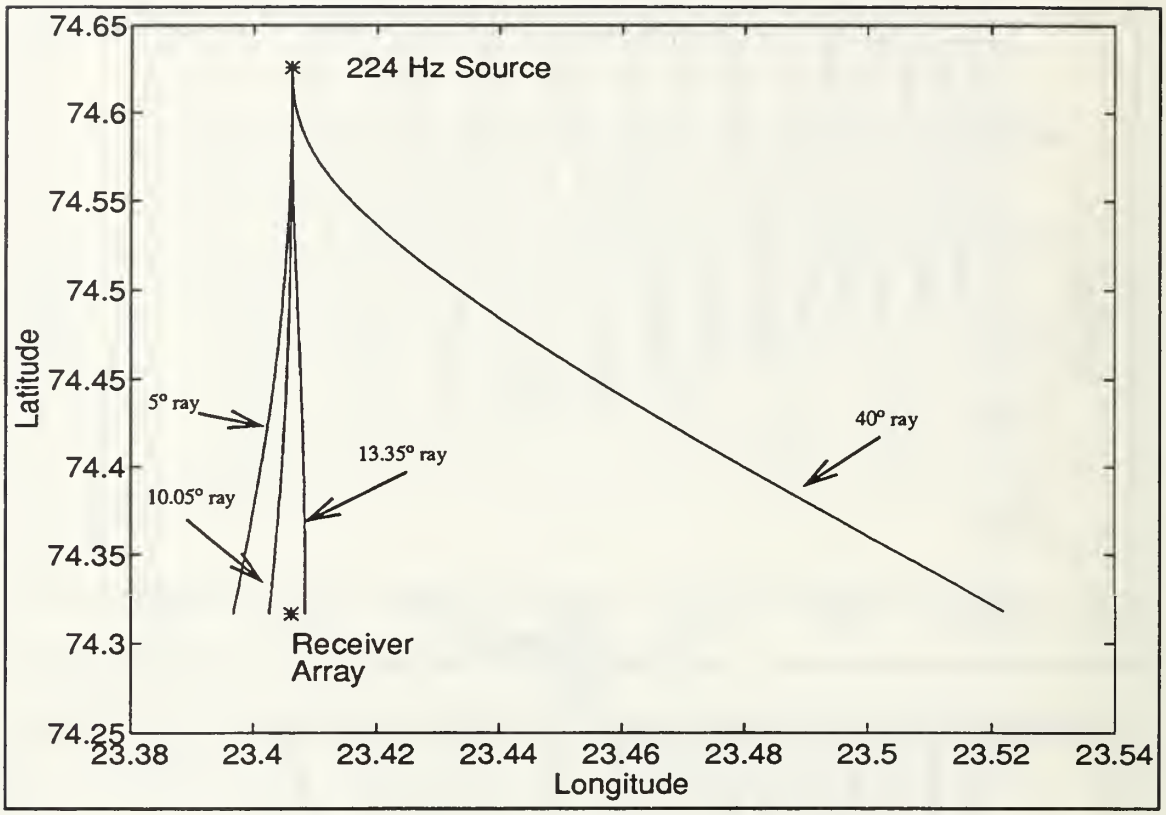

Figure 15. The amount of horizontal refraction experienced by the given rays is depicted in this overhead view of the ray paths. Note that this figure is not to scale but clearly shows that rays launched at shallow grazing angles are driven westward by the sound speed field whereas those rays launched at steeper angles are steered eastward by the bathymetry.

C. ARRIVAL STRUCTURE

To examine the arrival structure, various plots were made based on all of the rays traced. Figure 16 is a plot of arrival angle versus arrival depth. Both the 2-D and 3-D cases show similar forms in that the majority of the rays arrive at depths greater than 100 m. Those rays that are not completely surface-reflected and bottom-reflected, i.e., those rays with launch angles less than 13.35°, show a distinctive relationship between launch angle and arrival depth in that the minimum depth of arrival decreases with increasing launch angle. At a given depth, the eigenrays are those rays launched at the specific angles determined by the angle versus depth curve. In general, the number of eigenrays increases with depth.

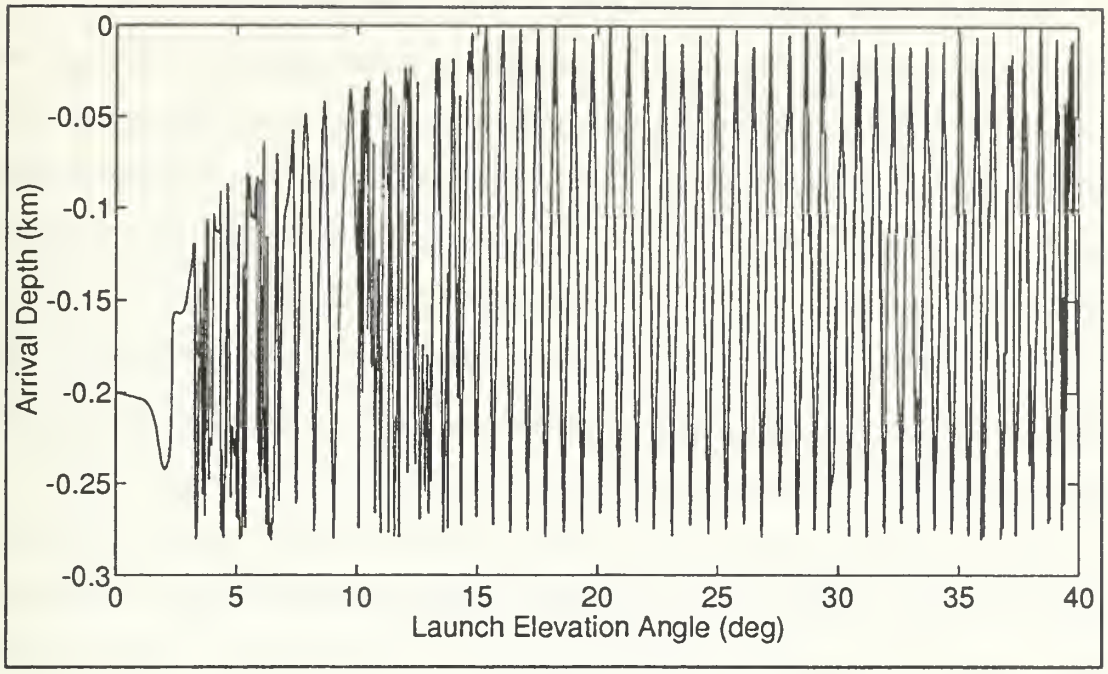

(a)

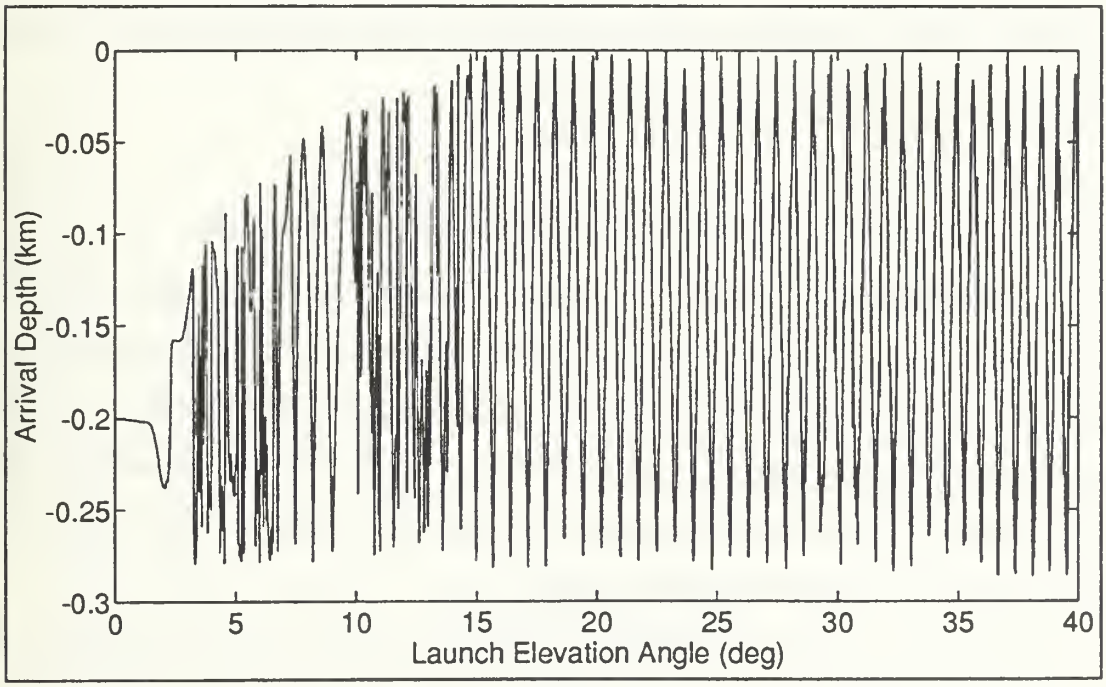

(b)

Figure 16. Arrival depth versus launch angle for the (a) 2-D environment and the (b) 3-D environment.

Figure 17 shows a plot of launch angle versus arrival time. In this figure one can see that the earliest arrivals were those rays launched at smaller angles. As the launch angle increases, so does the corresponding travel time. Note that for the 3-D case, the travel times for those rays launched at the steepest angles are a little less than those launched at the same angles in the 2-D case. This is likely due to the fact that the rays launched at steeper angles undergo more boundary interactions. As discussed earlier, the bathymetry in the 3-D case would tend to steer these rays towards the east, a region where sound speed is higher. From Figure 15, the ray launched at 40.00^{o} arrived at the receiver range approximately 6^{o} east of the line of sight, corresponding to a distance of about 3.6 km east of the array.

Figure 18 shows a plot of arrival depth versus arrival time. Arrivals less than 25 s (corresponding to shallow and moderate launch angles) show much more regularity than those later arrivals associated with steeper rays. The irregularities among the arrivals greater than 25 s indicate that the wave front has become distorted as a result of the numerous bottom interactions. The implications of this particular effect on the signal processing beamforming will be discussed later.

C. PLANE WAVE BEAMFORMED ARRIVAL STRUCTURE

This objective of this study is to provide a prediction of the plane wave beamformed arrival structure for the Barents Sea tomography transmission test. This prediction can be achieved by analyzing the arrival angle and time dependence of the eigenrays at the center of the array (located at a depth of approximately 195.8 m). An M.S. thesis study by Phil McLaughlin, LT, USN, has incorporated these predicted arrivals for the identification of the observed plane wave beamformed arrivals.

Figure 19 shows the arrival structures for both the 2-D and 3-D cases. There were 162 eigenrays identified in the 2-D simulation and 143 eigenrays in the 3-D case. A comparison of the arrival structures for the two simulations is given in Figure 20. It is interesting to note that for arrivals less than 25 s, both cases compare very well with each other. Again, these

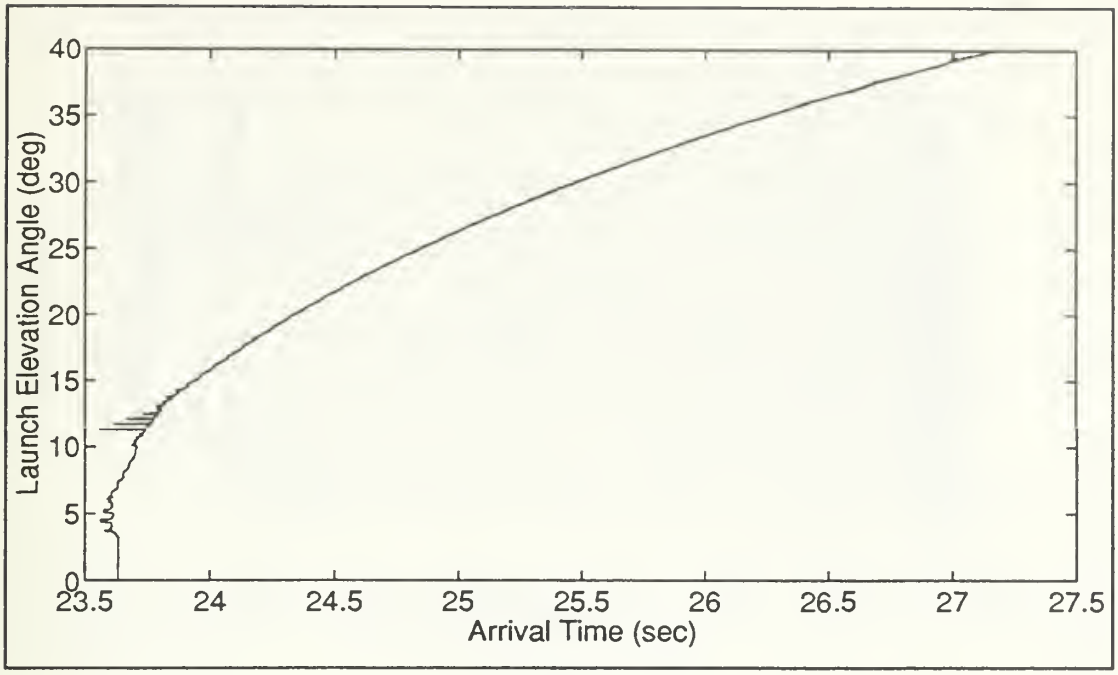

(a)

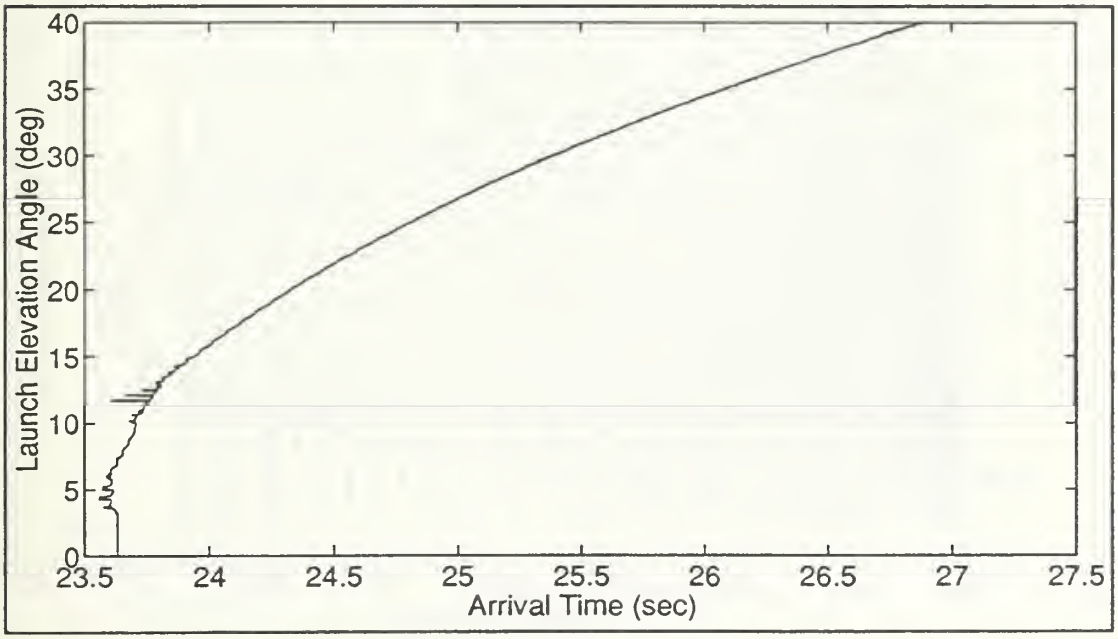

(b)

Figure 17. Launch angle versus arrival time for (a) propagation in a 2-D environment, and (b) propagation in a 3-D environment.

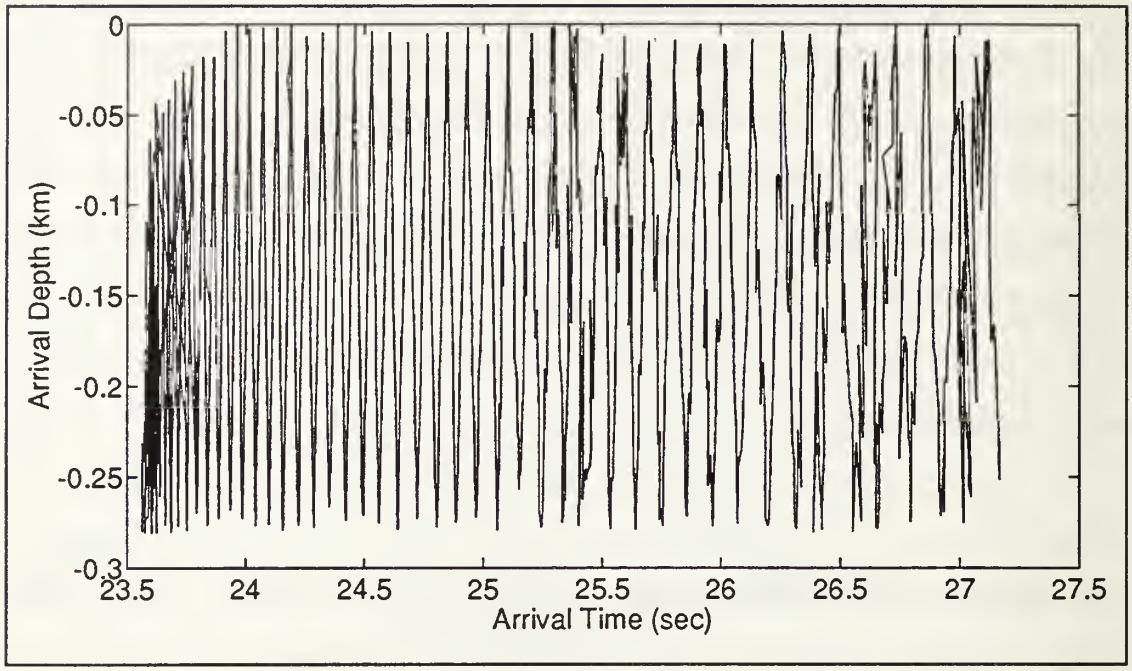

(a)

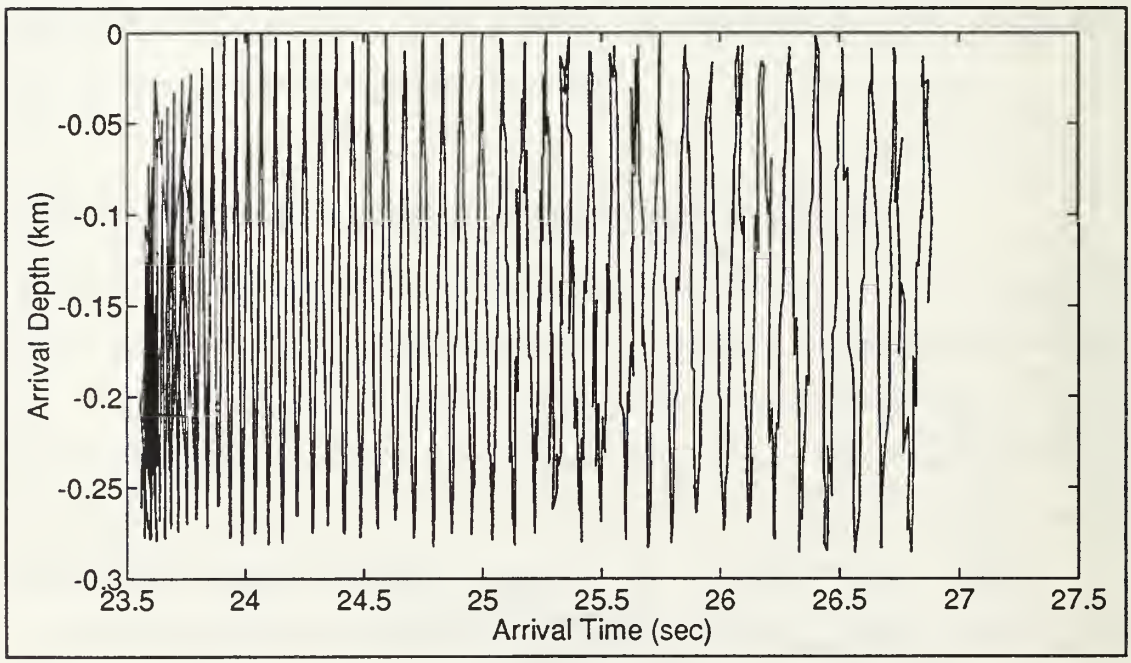

(b)

Figure 18. Arrival depth versus arrival time for (a) propagation in a 2-D environment, and (b) propagation in a 3-D environment.

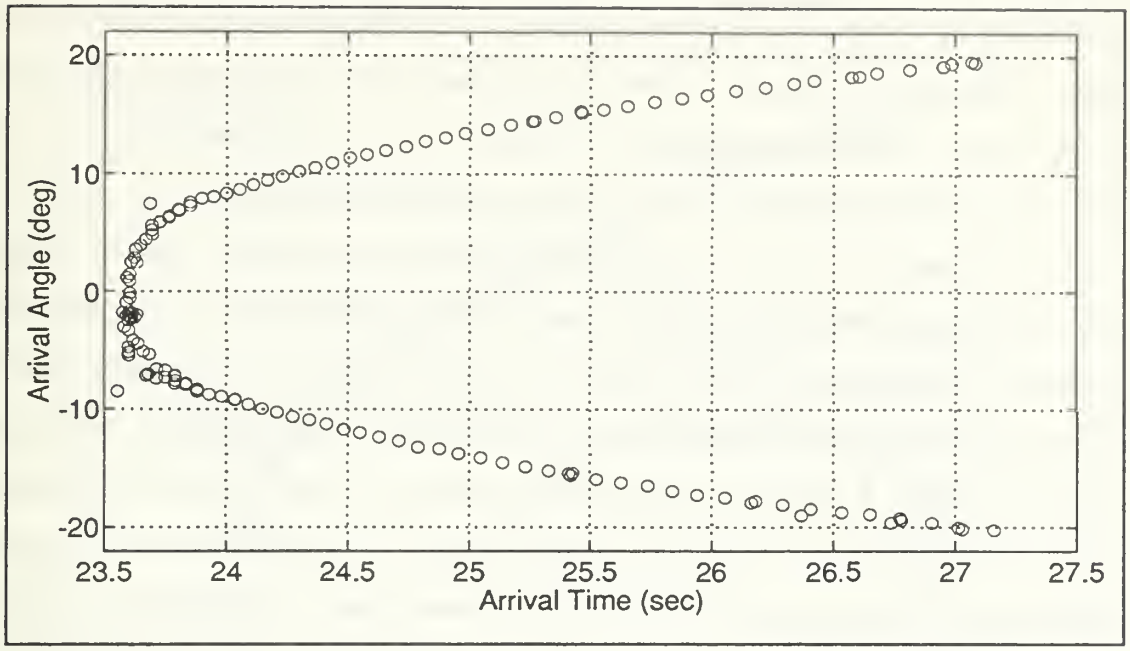

(a)

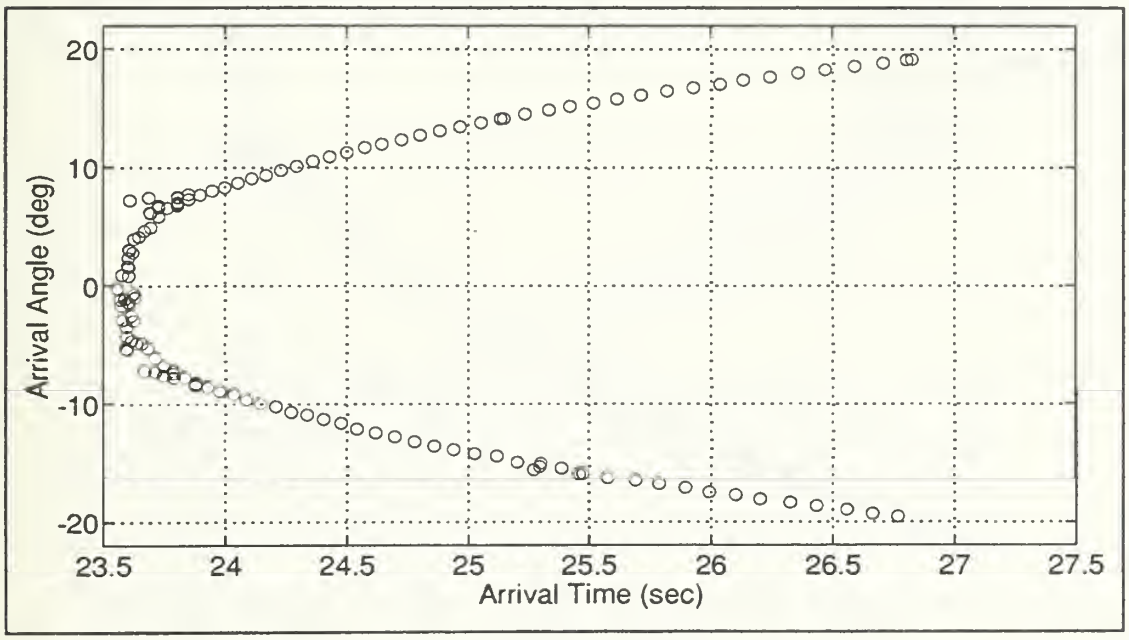

(b)

Figure 19. Channel 7 arrival angle versus arrival time for (a) propagation in a 2-D environment, and (b) propagation in a 3-D environment.

arrivals are associated with rays launched at low and moderate angles. After 25 s, however, the differences between the two cases gradually increase and the latest arrivals differ as much as 300 ms. These latter arrivals are associated with the steep angle rays which, through bottom interaction, undergo a significant amount of horizontal refraction. The result of the observed plane wave plane wave beamformed arrival structure is given in Figure 21 (Miller, et al., 1993). This figure shows the normalized arrival structure for plane wave beamformed data at one degree increments from -19.00^{o} to 19.00^{o}. The dark areas represent the peaks of the arrivals. Note that this data compares favorably with the predicted arrival structure. Figure 22 shows a plot of relative magnitude versus arrival time and arrival angle. Both cases show certain similarities in that the relative magnitude decreases with increasing arrival time. This dependence is primarily the result of surface scattering, and again, because the later arrivals are associated with steeper angles, they are thus subject to more boundary interactions, hence, greater losses. Based on the work by Emblidge (1991), mean wave heights of one meter were used in modeling sea surface roughness.

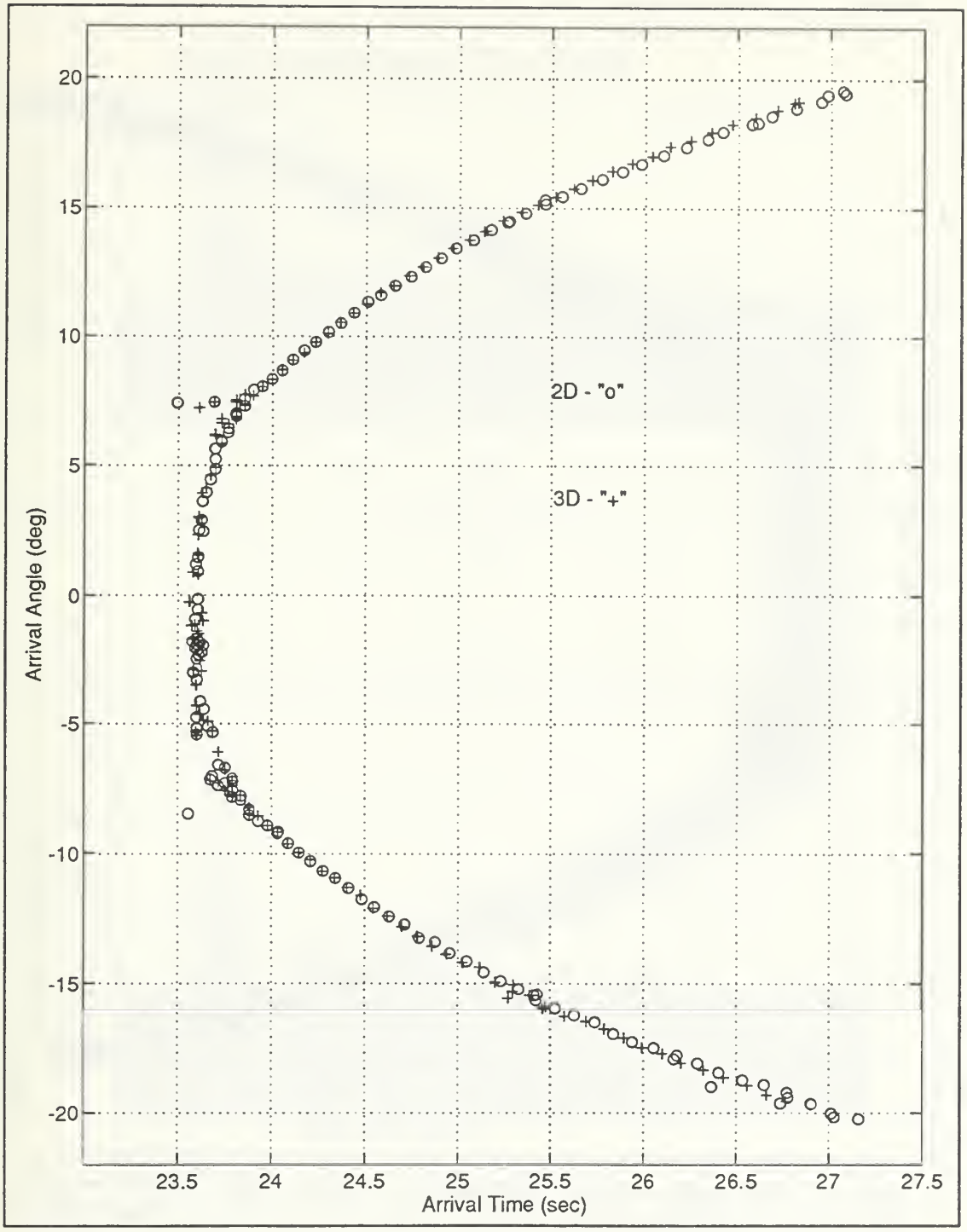

Figure 20. Channel 7 predicted plane wave beamformed arrival structure. (2-D results are represented by "o", 3-D results are represented by "+").

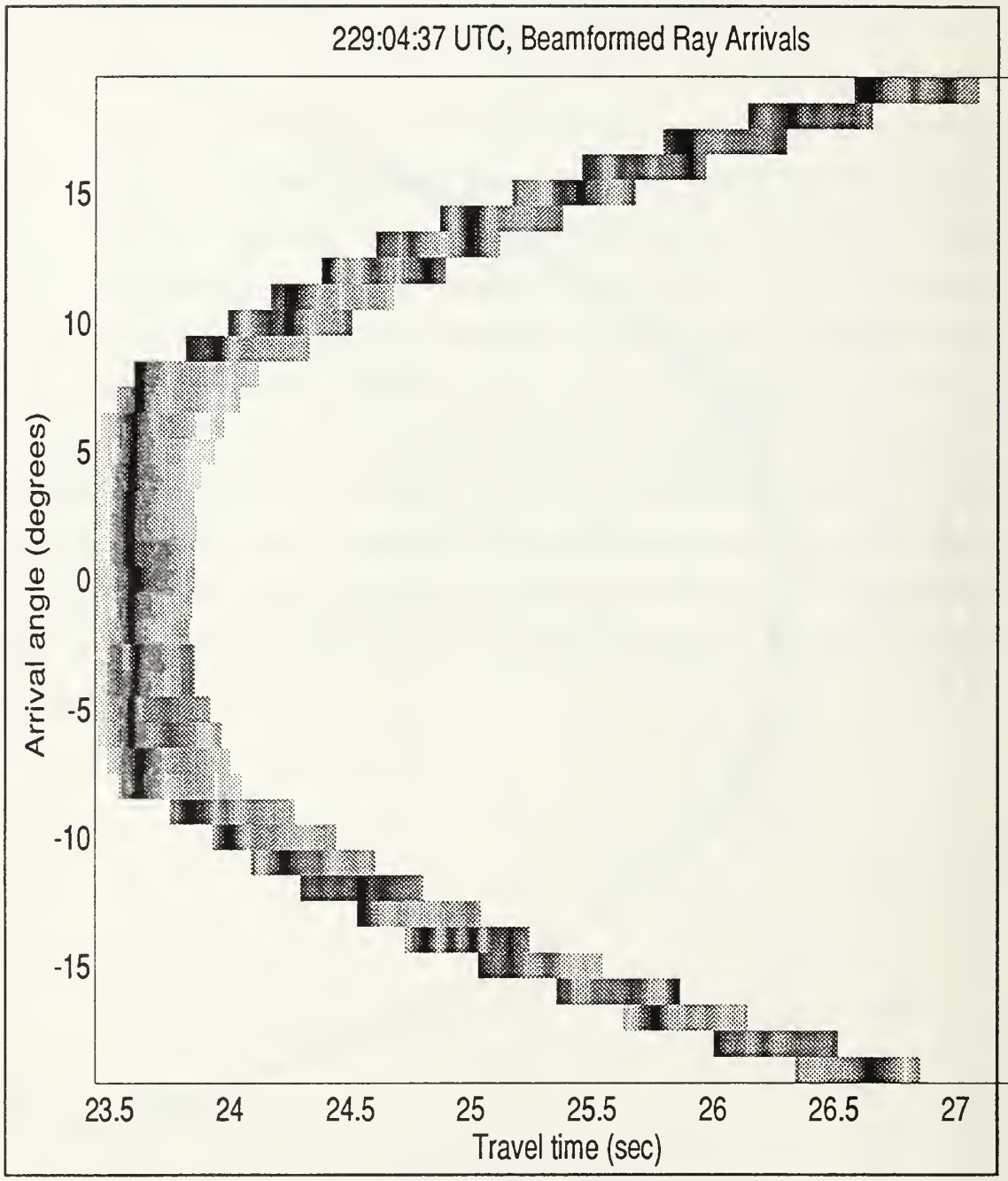

Figure 21. Coherent average of 28 sequences of length 3.9375 seconds for plane wave beamforming angles from -19 to 19 degrees in increments of one degree (from Miller, et al., 1993).

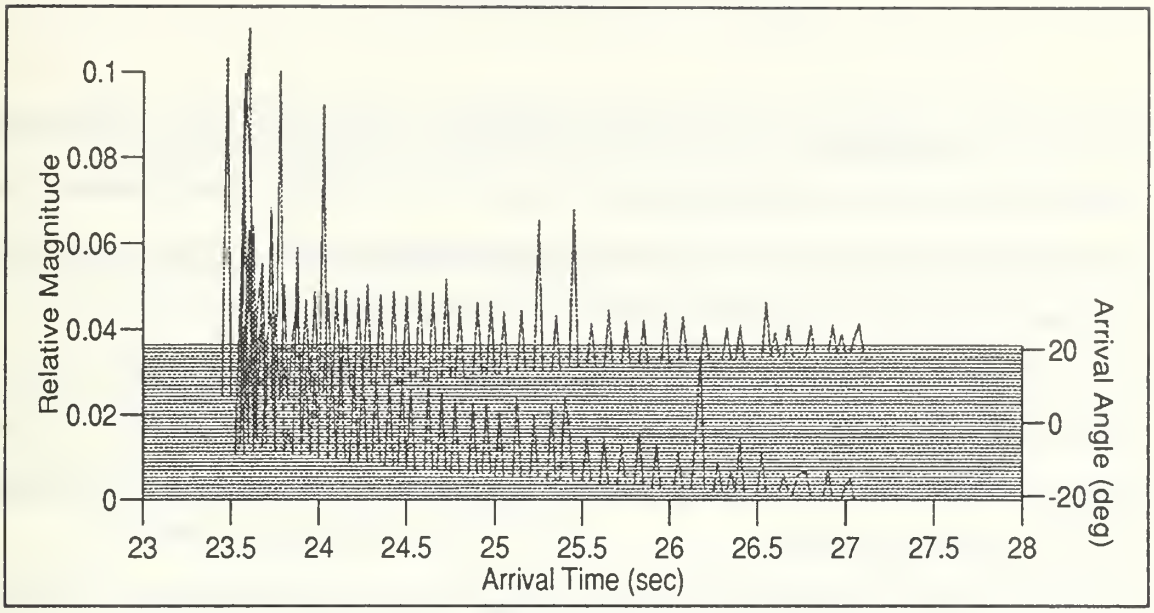

(a)

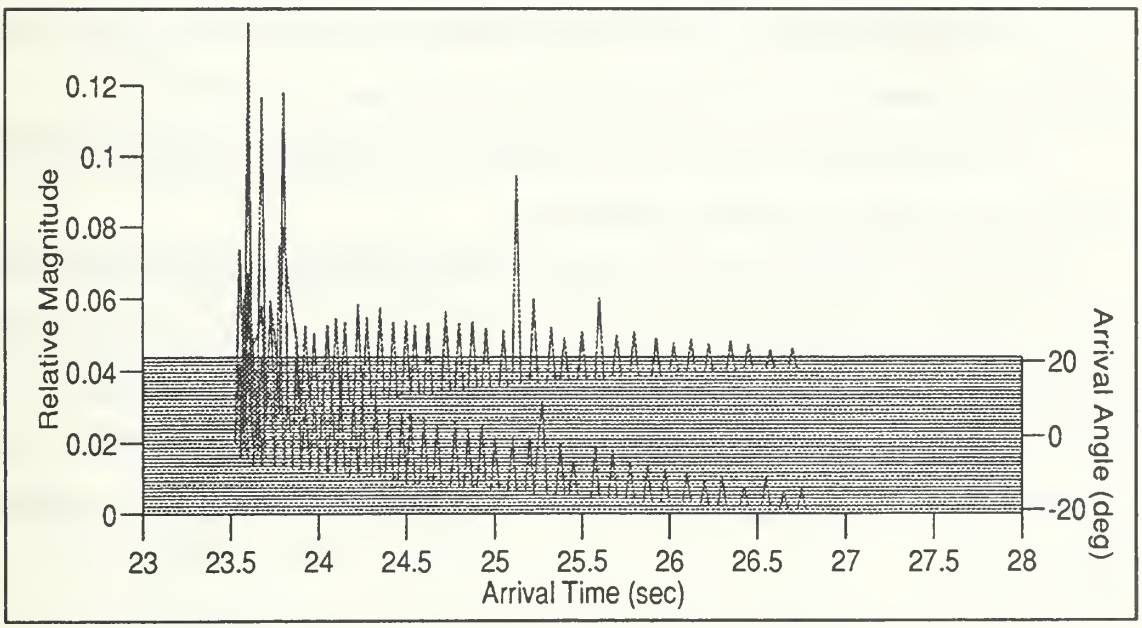

(b)

Figure 22. Relative magnitude of Channel 7 arrivals for (a) propagation in a 2-D environment, (b) propagation in a 3-D environment.

V. CONCLUSIONS

It was the objective of this thesis to employ a ray theory model to produce the predicted plane wave beamformed arrival structure for the 1992 Barents Sea tomography transmission test. Both a 2-D and 3-D modeled environment were used in an effort to determine the effects of horizontal refraction on the arrival structure.

For both cases, arrivals could be separated into two distinct groups:

1) Early Arrivals - those arrivals with travel times less than or equal to 25 s. These arrivals are associated with rays launched between 0.00^{o} and 28.00^{o} and have arrival angles between -14.00^{o} and 14.00^{o}.

2) Late Arrivals - those arrivals with travel times greater than 25 s. These arrivals are associated with launch angles greater than 28.00^{o} and have arrival angles between $\pm 15.00^{o}$ and $\pm 20.00^{o}$.

In both the 2-D and 3-D cases, the late arrivals showed a distortion of the wave front. In terms of signal processing implications, this could reduce the accuracy with which the travel time is estimated for the steep angle rays using plane wave beamforming.

As expected, in both cases, later arrivals exhibit significantly more loss than early arrivals due to numerous boundary interactions.

The effect of propagation in the 3-D environment appears to be prominent only in the late arrivals. This is primarily due to the nature of the bottom which is causing both wave front distortion and significant horizontal refraction for the very steep angle rays.

Most importantly however, this study has demonstrated that an acoustic ray theory model can be used to accurately predict the plane wave beamformed arrival structure for shallow water.

LIST OF REFERENCES

Barents Sea Polar Front Group, *Experimental Plan Barents Sea Polar Front Experiment August 1992,* May 1992. (Bourke, R.H., C.-S. Chiu, J.F. Lynch, J.H. Miller, R.D. Muench).

Brekhovskikh, L. and Yu. Lysanov, *Fundamentals of Ocean Acoustics,* Springer-Verlag Berlin Hiedelburg, New York,1982.

Clay, C.S. and H. Medwin, *Acoustical Oceanography*, John Wiley & Sons, New York, 1977.

Chiu, C.-S., Department of Oceanography, Naval Postgraduate School, Monterey, CA, Personal Communication, 1992-1993

Chiu, C.-S., J.H. Miller, and J.F. Lynch, "Inverse Techniques for Coastal Acoustic Tomography", submitted to the Proceedings of the 1993 International Conference on Theoretical and Computational Acoustics, July 1993.

Chiu, C.-S., A.J. Semtner, C.M. Ort, J.H. Miller and L.L. Ehret, "A ray variability analysis of sound transmission from Heard Island to California", accepted by the *Journal of the Acoustical Society of America: The Heard Island Experiment Special Issue*, 1993.

Elliott, J.M., *Simulation of Acoustic Multipath Arrival Structure in the Barents Sea,* Naval Postgraduate School Thesis, 1992.

Emblidge, J.M., *A Feasibility Study of Ocean Acoustic Tomography in the Barents Sea,* Naval Postgraduate School Thesis, 1991.

Jones, R.M., J.P. Riley and T.M. Georges, *HARPO a versatile three-dimensional hamiltionian ray-tracing program for acoustic waves in an ocean with an irregular bottom*, Wave Propagation Laboratory, NOAA, Boulder, Colorado, 457 pp., 1986.

Leong, H., *Features of the physical oceanographic conditions of the Barents Sea*, unpublished manuscript, 1991.

Miller, J.H., Department of Electrical and Computer Engineering, Naval Postgraduate School, Monterey, CA, personal communication, 1992-1993.

Miller, J.H., C.-S. Chiu and J. F. Lynch, "Signal Processing for Coastal Acoustic Tomography", submitted to the Proceedings of the 1993 International Conference on Theoretical and Computational Acoustics, August 1993.

Munk W., and C. Wunsch, *Ocean acoustic tomography: a scheme for large scale monitoring*, Deep Sea Res., v. 26, Part A, 123-161, 1979.

Newhall, A.E., J.F. Lynch, C.-S. Chiu and J.R. Daugherty, "Improvements in the three-dimensional raytracing codes for underwater acoustics, *Computational Acoustics*, v. I, 1987.

Norsk Polarinstitutt, Bathymetry Barents Sea, Chart No. 7421, Olso, Norway, 1986.

Urick, Robert J., *Principles of Underwater Sound*, 3rd ed. McGraw-Hill Book Co., New York, 1983.

INITIAL DISTRIBUTION LIST

1.	Defense Technical Information Center Cameron Station Alexandria, VA 22304-6145	2
2.	Librarian Code 52 Naval Postgraduate School 411 Dyer Road Monterey, CA 93943-5002	2
3.	Oceanography Department Code OC/Co Naval Postgraduate School 833 Dyer Road Monterey, CA 93943-5114	1
4.	Professor Ching-Sang Chiu Code OC/Ci Naval Postgraduate School 833 Dyer Road Monterey, CA 93943-5114	1
5.	Professor James H. Miller Code EC/Mr Naval Postgraduate School 833 Dyer Road Monterey, CA 93943-5114	1
6.	Office of the Oceanographer of the Navy Attn: Dr. Robert Winokur Naval Observatory 34th and Massachusetts Avenue NW Washington, DC 20390	1
7.	Commander Naval Oceanographic Command Stennis Space Center Bay St. Louis, MS 39539-5000	1

8. Dr. Thomas Curtin — 1
Office of Naval Research
800 North Quincy Street
Arlington, VA 22217-5000

9. LT John L. Mykyta — 1
Fleet Numerical Oceanography Center
7 Grace Hopper Avenue, Stop 1
Monterey, CA 93943-5501

10. Professor James F. Lynch — 1
Department of Applied Ocean Physics and Engineering
Woods Hole Oceanographic Institution
Woods Hole, MA 02543

11. Mr. Barry P. Blumenthal — 1
Office of Naval Research
800 North Quincy Street
Arlington, VA 22217-5660

12. Dr. Mohsen Badiey — 1
Office of Naval Research
800 North Quincy Street
Arlington, VA 22217-5000